*energies*

*Article*

# Assessment of Ground Regeneration around Borehole Heat Exchangers between Heating Seasons in Cold Climates: A Case Study in Bialystok (NE, Poland)

**Joanna Piotrowska-Woroniak**

HVAC Department, Bialystok University of Technology, Wiejska 45E, 15-351 Bialystok, Poland; j.piotrowska@pb.edu.pl

**Abstract:** Based on the experimental studies, the process of ground regeneration around the borehole loaded with brine-water heat pumps working exclusively for heating purposes in the period of four consecutive heating seasons in a cold climate was presented. The research was conducted in north-eastern Poland. The aim of the work is to verify the phenomenon of thermal ground regeneration in the period between heating seasons on the basis of the recorded data and to check whether the ground is able to regenerate itself and at what rate. It was noticed that the ground does not fully regenerate, especially during heating seasons with lower temperatures. In the analyzed period, from 22 September 2016 to 12 October 2020, the ground probably cooled irreversibly by 1.5 °C. In order to illustrate and evaluate the speed of changes in the ground, the one's profile with an undisturbed temperature field was presented for each month of the year. The presented results can be a very important source of information for the analysis of geothermal conditions occurring in the ground. They can be used to verify mathematical models and conduct long-term simulations that allow us to see the complexity of the processes taking place in the ground.

**Keywords:** ground thermal conductivity; thermal performance; extracted energy; borehole heat exchanger; BHE; ground-source heat pump; regeneration



**Citation:** Piotrowska-Woroniak, J. Assessment of Ground Regeneration around Borehole Heat Exchangers between Heating Seasons in Cold Climates: A Case Study in Bialystok (NE, Poland). *Energies* **2021**, *14*, 4793. https://doi.org/10.3390/en14164793

Academic Editors: Alessia Arteconi, Marcin Jewiarz and Krzysztof Mudryk

Received: 9 July 2021
Accepted: 3 August 2021
Published: 6 August 2021



## 1. Introduction

Climate change is a major challenge for the world community. European countries aim to achieve zero net emissions by 2050 [1,2]. Buildings, which account for up to 36% of final energy consumption, can make an important contribution to achieving this goal [3,4]. Clean and renewable energy resources are gaining popularity due to their advantages over fossil fuels, which have a significant impact on global warming and pollution. As one of the main options for replacing conventional energy sources, geothermal energy is becoming more and more attractive due to its wide availability, low operating costs, and low $CO_2$ emissions [5].

The design phase of ground source heat pump (GSHP) systems is extremely important as many of the decisions made at this stage may have an impact on the energy performance of the system as well as installation and operation costs [6,7]. Borehole heat exchangers (BHE) are the most frequently used devices in buildings due to their efficiency [8,9]. BHEs are a key technological component of geothermal energy systems, and much attention has been paid to modeling their behavior. The main technical challenge in designing geothermal heat exchanger systems is the ability to predict long-term temperature trends in groups of wells. This inevitably requires computer models implemented in design software or tools to simulate thermal systems [10,11]. Many studies look for a function describing the ground temperature profile, the most popular are those proposed by Kasuda et al. [12], which report a sinusoidal change in ground temperature at various depths as a function of average temperature. Most analytical and numerical methods are not always able to actually predict the temperature distribution in the ground. More information regarding the numerical methods and simulations used in the calculations of BHE and heat transfer in the ground can be found in [13–32]. In vertical arrangements, it is obvious to use single or double U-shaped heat exchangers, separated by longitudinal spacers. Sáez Blázquez et al. [33] investigated the effect of these components on overall BHE performance. Regarding the heat exchange process between the ground and the heat transfer fluid, it should be emphasized that the best results were obtained using a spiral-shaped pipe system. They noted the importance of using spacers in the U-shaped vertical tubes and that no improvements were found in the use of single or double U-tube configurations. Thanks to the laboratory results obtained from these studies, it is possible to determine the optimal pattern of behavior for entire vertical closed systems [33]. Neuberger and Adamovský [34] presented the results of operational monitoring, analysis and comparison of temperatures, power, and energy of antifreeze in the most commonly used low-temperature heat sources. The results of the verification showed that it was not possible to unequivocally define the most advantageous low-temperature heat source that meets the requirements for the efficiency of heat pump operation. In BHEs, the remainder of the well is filled with a grout filler, most often bentonite, quartz with sand, or just a mixture of water, in many northern European countries, in hard crystalline rock, BHEs are simply filled with groundwater, while in other cases usually, the BHE drill ring is cemented to ensure good thermal contact between the U-shaped or double U geothermal probes and the surrounding ground [35,36]. Due to the earthworks, the length of the geothermal heat exchanger must be properly calculated. Too little will cause excessive discharge and no time to regenerate it in the summer. Too many of them will generate unnecessary costs. Therefore, it is preferable to calculate the lower parameters of the heat source as accurately as possible. There are many attempts to solve this problem analytically and with the help of computer simulations [37–49], but so far there is no universal formula. Real measurement results are required for calculations and simulations. A series of studies [50–56] have been carried out to evaluate the efficiency of BHE in heat pump systems. All of these studies described the impact of BHE based on the evaluation of COP improvement in these systems. The Thermal Response Test (TRT) is a common procedure to characterize the thermal properties of the ground and the wellbore needed to design a shallow geothermal heat pump [57]. For this interpretation, the TRT measurements must be made under the specified boundary conditions; if any of its assumptions are invalid, the interpretation leads to an error in the final result [33,58]. TRT is especially needed in large scale installations where an improper BHE design will mean poor system performance if the system is too small or unjustified cost overruns if it is oversized. TRT is based on the thermal response of a heat exchanger to a constant heat injection or extraction pulse lasting several days. The most significant variables measured with the TRT are the temperature of the heat transfer fluid at the inlet and outlet of the heat exchanger, measured during the execution of the test. By comparing these experimental data with the model describing the heat exchange between the liquid and the ground, it is possible to estimate the thermal properties of the ground [57,59–62]. Sáez Blázquez et al. [63] proposed a new experimental device that provides an inexpensive, less time-consuming, and reliable approach to measuring thermal conductivity. This approach may replace or supplement well-known but expensive methods such as the thermal response test (TRT). Bae et al. [64] evaluated the thermal performance of different types of BHE pipes using the Thermal Response Test (TRT) under the same field and test conditions and found that the average thermal resistance of the well could be an important factor in TRT, but the effect of the increased thermal conductivity of the pipe material itself was not significant. Another important point is that the presence of groundwater advection can greatly increase heat transfer and speed up the possibility of ground restoration, as studied by Serageldin et al. [65], Lei et al. [2], Park et al. [66], and Sakata et al. [67].

Sliwa and Rosen [68] presented an overview of natural and artificial methods of regenerating heat resources for BHE and took into account some of the natural methods of ground regeneration, such as: groundwater flow, solar energy falling to the surface (wind and also frost), heat transfer from sides of the BHE space, heat transfer from the bottom of the BHE space. Solar radiation on the earth's surface and warm air/ambient wind are two important heat sources for BHE fields. These sources are especially important when the depth of the well is not great. In deep BHEs, the regeneration of heat from solar radiation and atmospheric air is not so significant, and its importance decreases with increasing depth. The thermal resistance of the ground has a great influence on the heat transfer between the heat carrier and the ground. The second group of heat sources for resource regeneration is geothermal heat from the surroundings and from under the BHE field. When the geothermal source heat pump (GSHP) has only this heat source regeneration system, conduction of heat from the ground itself may not be sufficient, and the temperature of the BHE field may drop from year to year, heat renewal in such heat exchanger fields is incomplete, after several years of temperature drop. The temperature takes a low value at which heat from the vicinity of the BHE field can additionally dissipate to this field. Convection is the third group of natural heat sources for the regeneration of the BHE field. Sensitivity of loop outlet temperatures and heat transfer rates to hydrogeological, systemic, and meteorological factors. Where there is groundwater flow, the mass flow may be accompanied by heat transfer. Natural methods of heat regeneration may result in full or only partial temperature regeneration. When full temperature renewal is not achieved due to additional heat resources, it is necessary to use artificial heat sources. Miglani et al. [69] described a methodology for optimizing the building's energy system, including a detailed BHE-based GSHP thermal model. The novelty of their model is that it enables the study of dynamic changes in ground temperature during operation. In addition, a model of thermal solar collectors was also included, which allows the study of solar ground regeneration in the short, and long term. The results show that the ground temperature drops significantly in the short term, and that solar regeneration due to excess heat in summer brings the temperature back above the initial temperature. However, due to insufficient regeneration in the long term, the ground temperature continues to drop. Zhao et al. [70] investigated GSHP ground temperature distributions with different degrees of heat recovery. Compared to conventional GSHP, those with heat recovery maintained constant ground temperature and thermal imbalance factors during extended use, especially in hot summer and cold winters areas.

The aim of the work is to verify the thermal regeneration phenomenon of the ground in the period between heating seasons on the basis of the recorded data. This period should be sufficient for the lower heat source temperature to return to the state before the previous heating season. However, if the temperature of the heat source drops consistently, it may be necessary to support regeneration, e.g., with solar collectors in the summer. The available literature, e.g., [54,71–77], shows that in cold regions it seems necessary for long-term use.

## 2. Materials and Methods

### *2.1. Experimental and Measuring Site*

The study of the ground regeneration process around the selected well was carried out in the north-eastern part of Poland in Bialystok on the campus of the Bialystok University of Technology. The city belongs to the "Green Lungs of Poland". The geographic coordinates of the explored well and the entire lower heat source are: longitude from $23°9'0.72''$ to $23°9'14.06''$ and latitude from $53°7'1.9''$ to $53°7'8.94''$. According to the Köppen-Geiger climatic classification, the research site is located in the area of temperate continental climate, designated as Dfb [78].

The analysis of the course of ground regeneration around the well covers the following heating seasons: 2016/2017, 2017/2018, 2018/2019, and 2019/2020. The research was carried out from 22 September 2016 to 12 October 2020. The article presents the evaluation of ground regeneration on the example of one well, which was loaded with BHE work.

The standard heating season in this region of Poland lasts 232 days, and the regeneration period is 133 days, begins around 11 May, and lasts until around 20 September. The number of heating degree days (HDDs) in the standard heating season based on the multi-year outdoor temperatures (1991–2020) is 3496.1 days/K year, an internal air temperature in the heating zone of $t_w$ = 18 °C. Unfortunately, not every heating season is the same. Recent years have been characterized by very mild winters and hot summers (e.g., 2018, 2019), compared to the statistical multi-year climatic conditions.

The characteristic climatic conditions for the area where the study of ground changes during the period of its regeneration in 2016–2020 was carried out and the statistical climatic conditions from the multi-year 1991–2020 are shown in Tables 1 and 2.

**Table 1.** Average outside air temperature from April to September for the area covered by BHE regeneration studies (Data from the Institute of Meteorology and Water Management) [79].

| Month | Average Outside Air Temperature [°C] | | | | | |
|---|---|---|---|---|---|---|
| | Statistical 1991–2020 | 2016 (2015/2016) * | 2017 (2016/2017) * | 2018 (2017/2018) * | 2019 (2018/2019) * | 2020 (2019/2020) * |
| April | 7.9 | 8.0 | 6.3 | 11.7 | 8.9 | 7.1 |
| May | 13.1 | 14.5 | 12.9 | 16.7 | 12.9 | 10.8 |
| June | 16.4 | 17.5 | 16.2 | 18.0 | 20.8 | 18.7 |
| July | 18.4 | 18.3 | 17.1 | 19.8 | 17.3 | 17.6 |
| August | 17.5 | 16.9 | 17.6 | 19.2 | 17.8 | 18.7 |
| September | 12.6 | 13.5 | 13.2 | 14.6 | 13.0 | 14.4 |
| Average | 14.3 | 14.8 | 13.9 | 16.7 | 15.1 | 14.6 |

*—heating season.

**Table 2.** The minimum temperature at the ground from April to September for the area covered by BHE regeneration studies (Data from the Institute of Meteorology and Water Management) [79].

| Month | Minimum Temperature Near the Ground [°C] | | | | | |
|---|---|---|---|---|---|---|
| | Statistical 1991–2020 | 2016 (2015/2016) * | 2017 (2016/2017) * | 2018 (2017/2018) * | 2019 (2018/2019) * | 2020 (2019/2020) * |
| April | −8.1 | −5.8 | −8.0 | −6.7 | −8.7 | −7.8 |
| May | −3.8 | −1.1 | −3.2 | 0.5 | −6.3 | −3.9 |
| June | 0.7 | −1.0 | −0.4 | −0.6 | 5.4 | 2.2 |
| July | 3.8 | 6.7 | 4.1 | 8.7 | 2.6 | 4.2 |
| August | 2.3 | 2.6 | 3.4 | 3.8 | 5.9 | 5.6 |
| September | −3.1 | −1.6 | −2.7 | −3.2 | −3.8 | −1.2 |
| Average | −1.4 | 0.0 | −1.1 | 0.4 | −0.8 | −0.2 |

*—heating season.

The ground temperature changes with depth, and the most intense changes occur in the subsurface layers, where the temperature change is influenced by weather factors, e.g., solar radiation, rainfall, humidity, or type of coverage.

A statistical measure describing the heat demand in a building is the number of HDDs in the heating season, which determines the energy consumption for heating buildings, and thus the intensity with which the lower heat source is used. On the basis of the calculated value of the number of HDDs, it is possible to compare successive heating seasons or refer to the standard multi-year heating season, which includes average outside air temperatures and the standard number of heating days in a given month.

In the work, in order to be able to compare the tested heating seasons, the number of HDDs for each of them was determined based on the relationship (1):

$$Sd(t_w) = \sum_{i=0}^{12} [t_w - t_e\ (i)] \cdot L_d\ (i) \quad for \quad t_e\ (i) < t_w \tag{1}$$

where:

$Sd(t_w)$—number of degree-days calculated for each year, [day/K·year],

$t_w$—average temperature of indoor air in the heating zone, accepted for calculations established 18°C, [°C]

$t_e\ (i)$—average monthly temperature of outdoor air for the particular year, [°C]

$L_d\ (i)$—number of heating days in the particular month for each year, [day].

Table 3 contains the number of HDDs calculated according to the Equation (1) that characterize a given heating season. The duration of the heating season is closely related to the regeneration period of the lower heat source. The longer the heating season, the shorter the period of ground regeneration around the exploited well, which was loaded with heat pumps work during the heating season.

**Table 3.** Characteristics of the heating season based on the number of HDDs.

| Years of the Heating Season | The Number of HDDs $S_d$ [Day/K·Year] | Average Annual Outside Air Temperature [°C], [79] |
|---|---|---|
| 2016/2017 | 3276.4 ↑ | 7.2 |
| 2017/2018 | 3174.1 | 8.8 |
| 2018/2019 | 3131.0 | 8.7 |
| 2019/2020 | 2651.4 ↓ | 9.2 |
| 1991—2020 | 3496.1 | 7.7 |

The shortest heating season was the 2019/2020 one, where the number of HDDs was 2651.4 day/K·year. It was characterized by the highest outside air temperatures in the heating season. The lowest outside temperature and the highest number of HDDs were characteristic of the 2016/2017 heating season.

The borehole selected for analysis with the 100 m deep working BHE placed in it is one of 52 working wells [80]. The GSHP installation based on 52 BHEs is operated solely for heating purposes for the building of the Bialystok University of Technology.

The analyzed BHE is a U-type exchanger and was made of PE-Xa cross-linked polyethylene with a diameter of 40 × 3.7 mm. The outer diameter of the borehole is 160 mm. The annular space between the BHE pipes and the well's walls was filled with a mixture of bentonite mixed with the spoil. The probe is located at a distance of 10 m from other vertical geothermal probes. All wells are spaced at equal 10 m intervals. The probe is 100 m deep and filled with an aqueous solution of propylene glycol, which is a heat carrier with the following parameters: concentration 39%, density 1038 kg/m$^3$, and specific heat 3.38 kJ/(kg K).

The land on which the BHE boreholes were drilled is covered with grass.

At the design stage, each BHE assumed a flow of 0.852 m$^3$/h [81], while the actual flows set on the rotameters during BHE operation are from 0.9 m$^3$/h to 1.9 m$^3$/h [80]. The maximum well power determined during the tests using the TRT test was 3.54 kW, with the operating time of the compressors up to 2000 h/year. Experimental measurements in 2018 and 2019 showed that the tested BHE wells during their operation did not reach their maximum power of 3.54 kW, determined by the TRT test, and the operating time of heat pump compressors exceeded 2000 h/year [80].

### 2.2. Ground Profile

The area where the studied BHE well is located is within the East European Platform.

Figure 1 shows the hydrogeological map with the BHEs location area marked; a better quality map is available on the website [82]. The area on which 100 m drillings were made in accordance with the presented map (Figure 1) does not have a designated usable aquifer and additionally, according to the map, it is located in the area of a depression cone caused by the exploitation of groundwater.

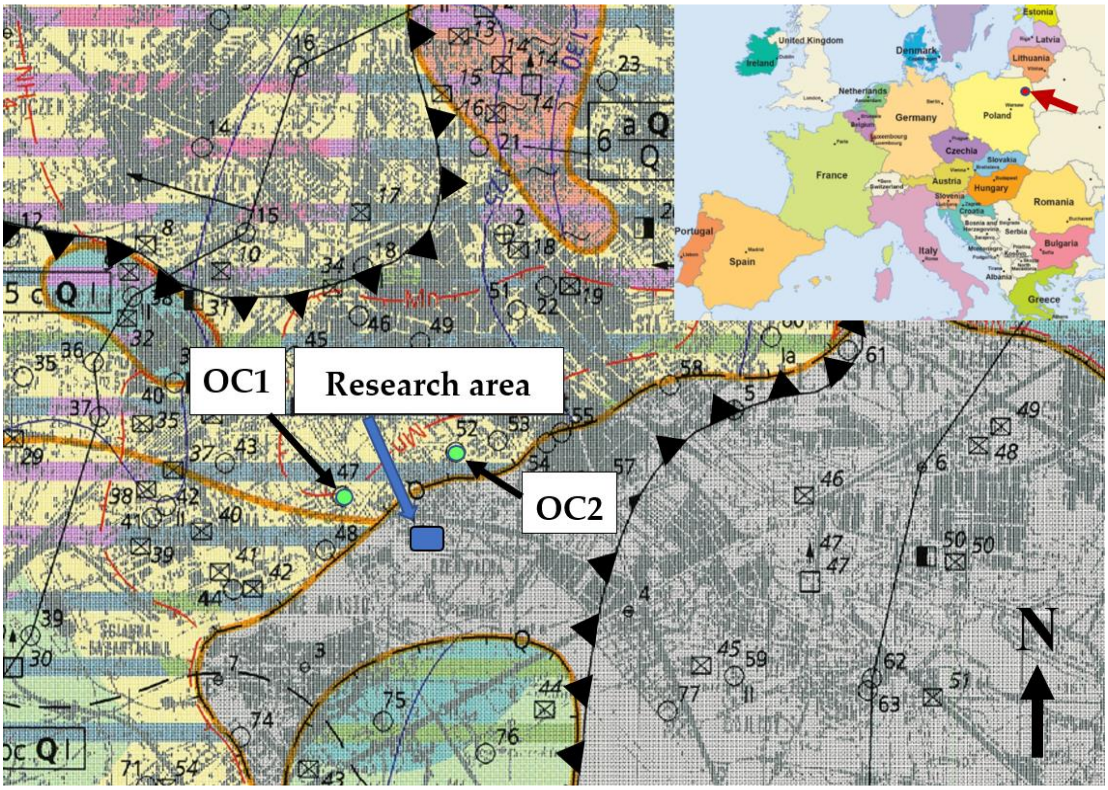


*Markings on the map:*

| | | | | | |
|---|---|---|---|---|---|
| | – | Research area of the phenomenon of ground thermal regeneration. | | | |
| | – | OC1—groundwater well for emergency purposes intake 62 m a.s.l. deep;<br>OC2—groundwater well for emergency purposes intake 195 m a.s.l. deep. | | | |
| | – | No designated aquifer. | | | |
| | – | A depression cone caused by the exploitation of groundwater. | | | |
| Aquifer—potential capacity of a drilled well, [m$^3$/h]: | | | | | |
| | – | 10–30 | | – | 50–70 |
| | – | 30–50 | | – | > 70 |

**Figure 1.** Hydrogeological map with the BHE regeneration research area marked (scale 1: 50,000) [82], (Red Arrow—location of the city of Bialystok on the map of Poland).

The geological profile of the ground-based on the documentation of the excavated material obtained during drilling [83] is as follows: at a depth of up to 2 m below ground level (b.g.l.) there is native ground, from 2 m to 4 m b.g.l., horizontal dry clay, 4 m to 12 m b.g.l., saturated sand and gravel, from 12 m to 40 m b.g.l., wet-humid, from 40 m to 45 m b.g.l. there are silts, from 45 m to 100 m b.g.l. there are the clay, moist-moist layers.

In the vicinity of the analyzed area, there are two groundwater wells for emergency purposes, OC1 and OC2, for which the hydrogeological conditions are known. The wells are marked in green in Figure 1. The measurement well OC1 has a defined bottom of the aquifer at a depth of 60 m above sea level (a.s.l.), and the top at a depth of 52 m a.s.l., while in the OC2 one the bottom of the aquifers is at depths of 59 m a.s.l., 118 m a.s.l. and 195 m a.s.l., and the top is at 36 m a.s.l., 104 m a.s.l., and 188 m a.s.l. [83].

Therefore, there is a high probability that the aquifer may exist at a similar depth for the area under investigation. However, it is uncertain whether the existing aquifer covers the entire area of the ground heat source and all the boreholes, or only a part of it because, according to Figure 2 (a better quality map is available on the website [82]), the borehole site is located in a place where the first aquifer is characterized by a significant diversification of the conditions of occurrence and properties of the aquifers. The water table is discontinuous and variable, and it can occur at different depths.

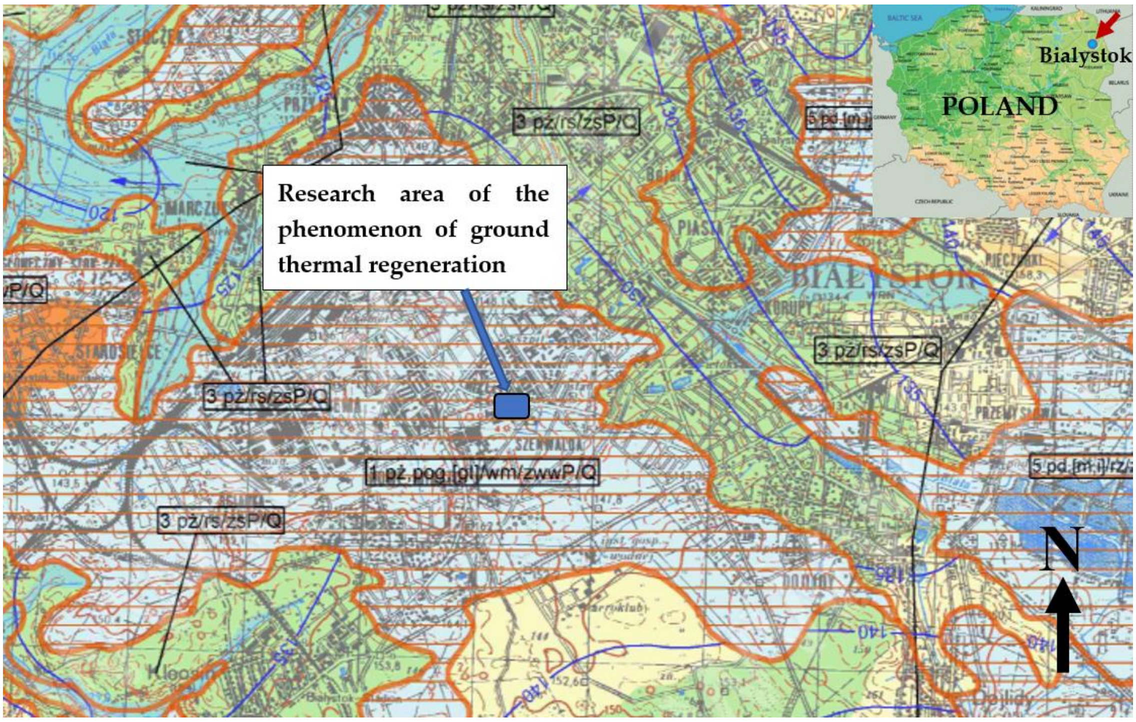


*Markings on the map*:

| | | | | | | | | |
|---|---|---|---|---|---|---|---|---|
| | – | Research area of the phenomenon of ground thermal regeneration. | | | | | | |
| | – | The area of occurrence of the first aquifer with significantly different occurrence conditions and properties of aquifers. The water table is discontinuous and of a changeable nature. | | | | | | |
| Depth to the first aquifer is given in meters above sea level (m a.s.l.): | | | | | | | | |
| | – | <1 | | – | 2–5 | | – | 5–20 |
| | – | 1–2 | | – | 5–10 | | | |

**Figure 2.** Hydrogeological map of the occurrence of the first aquifer with different conditions of occurrence of aquifers with the marked area of ground regeneration research around BHEs (scale 1:50,000) [82].

The most important parameters characterizing the thermal properties of the ground are: thermal conductivity coefficient, the heat capacity of the ground, and thermal diffusivity.

Table 4 presents the geological profile of the 100 m tested borehole along with the thermal characteristics of the ground layers and the location of temperature sensors at particular depths.

**Table 4.** The geological profile of the ground and the thermal characteristics of the ground lithologies have been assigned according to the EED software database [83,84].

| No. | Lithology [83] | Layer Top Bottom [83] [m.b.g.l.] | | Percentage of Total Thickness [%] | Volumetric Specific Heat $C_v = \rho \times C_p$ [MJ/(m$^3$·K)], [84] | Thermal Diffusivity a $\times 10^{-6}$ [m$^2$/s] | Number of Temperature Sensors Placed |
|---|---|---|---|---|---|---|---|
| 1 | Native ground | 0 m | 2.0 m | 2 | 1.4 | 0.36 | 7 pcs |
| 2 | Clay dry | 2.0 m | 4.0 m | 2 | 1.6 | 0.41 | 3 pcs |
| 3 | Sand and Gravel, saturated | 4.0 m | 12 m | 8 | 1.62 | 0.51 | 8 pcs |
| 4 | Clay, moist-wet | 12 m | 40 m | 28 | 2.4 | 0.65 | 6 pcs |
| 5 | Muds | 40 m | 45 m | 5 | 2.5 | 1.35 | 1 pcs |
| 6 | Clay, moist-wet | 45 m | 100 m | 55 | 2.4 | 0.65 | 5 pcs |

The weighted-average coefficient of volumetric heat capacity of the ground [MJ/(m$^3$·K)] was determined by the computational method as the weighted average of the individual layers of ground in the borehole, taking into account the share of a given layer in the entire structure of a 100-m borehole from the dependence (2):

$$Cv_{avg} = (0.02 \cdot Cv_1 + 0.02 \cdot Cv_2 + 0.08 \cdot Cv_3 + 0.28 \cdot Cv_4 + 0.05 \cdot Cv_5 + 0.55 \cdot Cv_6), \ \left[\mathrm{MJ}/\left(\mathrm{m}^3 \cdot \mathrm{K}\right)\right] \quad (2)$$

where: $Cv_n$—recommended coefficient of thermal capacity of a given layer of ground in the well [MJ/(m$^3$·K)], according to Table 4.

The calculated weighted average heat capacity of the ground in the tested well is $Cv_{avg}$ = 2.31 MJ/(m$^3$·K). The ground thermal conductivity coefficient, in accordance with the ground profile presented in Table 4, is λ = 1.76 W/(m·K) ± 0.03 W/(m·K). This coefficient was determined on the basis of the TRT test performed by an external company [80,81], it covers all ground layers.

The last parameter that allows describing of the ground in terms of its thermal properties is thermal diffusivity. Thermal diffusivity a [m$^2$/s], also called temperature conductivity, determines the ability of the ground to equalize the temperature, and its value depends on the type and moisture of the ground. There is a strong relationship between ground moisture and the value of the thermal conductivity coefficient. The lowest values of thermal diffusivity are found in dry ground, where the thermal diffusivity is, for example, for sand, dry $0.29 \times 10^{-6}$ m$^2$/s. The increase in thermal diffusivity occurs most often with the increase in thermal conductivity of the ground. On the other hand, a decrease in ground diffusivity is observed when the increase in heat capacity with humidity is greater than the thermal conductivity of the ground [85]. Table 4 shows the calculated thermal diffusivity for individual ground layers based on the relationship (3):

$$\mathrm{a}_{\ n} = \left(\frac{\lambda_n}{Cv_n}\right) \cdot 10^{-6}, \left[\frac{\mathrm{m}^2}{\mathrm{s}}\right] \quad (3)$$

where: $\lambda_n$—thermal conductivity coefficient of a given ground layer, [W/(m·K)], $Cv_n$—average coefficient of heat capacity of ground in a given layer [MJ/(m$^3$·K)].
wherein:

$$Cv_n = \rho \cdot C_p, \left[\frac{\mathrm{MJ}}{\mathrm{m}^3 \cdot \mathrm{K}}\right] \quad (4)$$

where: $\rho$—density [kg/m$^3$], $C_p$—specific heat [MJ/(kg·K)].

The thermal diffusivity of the ground layers in the tested well ranges from $0.49 \times 10^{-6}$ m$^2$/s to $0.96 \times 10^{-6}$ m$^2$/s.

In terms of numbers, the thermal diffusivity of the regenerated ground is equal to the temperature change rate $\frac{\partial \mathrm{T}}{\partial \tau}$ in a given soil layer, caused by a unit change in the temperature gradient. After transforming the heat conduction equation [86,87] in the form (5):

$$\frac{\partial \mathrm{T}}{\partial \tau} = \frac{\partial}{\partial \mathrm{x}}\left(a \frac{\partial \mathrm{T}}{\partial \mathrm{x}}\right) + \frac{\mathrm{q}_v}{\mathrm{C}_v}, \quad (5)$$

assuming that during the ground regeneration process, it is possible to assume $\mathrm{q}_v = 0$, we obtain the relationship (6) describing the thermal diffusivity:

$$a = \frac{\partial \mathrm{T}}{\partial \tau}\left(\frac{\partial \mathrm{T}}{\partial \mathrm{x}}\left(\frac{\partial \mathrm{T}}{\partial \mathrm{x}}\right)\right)^{-1}, \ \left[\frac{\mathrm{m}^2}{\mathrm{s}}\right] \quad (6)$$

where: T—temperature, τ—time, x—location coordinate (distance from the ground surface), $\mathrm{q}_v$—heat source efficiency, assumed $\mathrm{q}_v = 0$, $Cv_n$—volumetric heat capacity of the ground.

The weighted average coefficient of thermal diffusivity of the ground for the entire tested well is $0.76 \times 10^{-6}$ m$^2$/s.

At the Bialystok University of Technology 52 boreholes were drilled, in each of them there is a 100-m deep BHE, which is the lower heat source for two brine-water heat pumps with a total heating power of 234.4 kW working exclusively for heating the building. During the heating season, a BHE with a design maximum power of 3.54 kW is operating in the well [81].

*2.3. Measurement Methodology*

A 100-m custom-made measuring probe equipped with 30 digital temperature sensors was used to monitor changes in the ground temperatures around the BHE located in a 100-m depth borehole. Dallas Semiconductor DS18B20 sensors (Maxim Integrated Products, San Jose, CA, USA) were used, which were placed in a protective, tight, and waterproof housing. In order to increase the reliability of the measurement system, temperature sensors are placed on four 1-Wire buses, not just on one bus. Each 1- Wire bus has 8 or 7 digital DS18B20 sensors arranged alternately [88,89]. Electronic temperature sensors along the entire length of 100 m of the measuring probe are placed at the following distances from each other (see Table 4): on the first-meter section of the measuring probe every 0.2 m; in the section from 1 m to 3 m every half meter; in the section from 3 m to 13 m every one meter; in the section from 13 m to 15 m every two meters; on the section from 15 m to 30 m every five meters and on the section from 30 m to 100 m every ten meters (according to the concept of Piotrowska-Woroniak, Gajewski) [89].The measuring sensors are integrated with the SCADA (Supervisory Control and Data Acquisition) system that enables visualization, data collection, and supervision of the measurement and technological processes in the lower heat source. The measurement probe was placed approximately 10–15 cm from the BHE and inserted into the well along with the vertical ground probe during drilling work. Before starting the measurements, the sensors were calibrated with an accuracy of ±0.1 °C. Temperature measurements are carried out by means of continuous daily recording with the recording frequency every 300 s.

The second, the same probe with 30 temperature sensors type DS18B20 is used to measure the temperatures in the ground with intact structure. In this way, the temperature of the ground is controlled in a state of undisturbed natural thermal equilibrium, which may be disturbed, for example, by operating BHEs during the heating season. The measuring probe is placed at a distance of 9.2 m from the well being tested. The parameters of the used temperature sensors are presented in Table 5.

**Table 5.** The parameters of the Dallas Semiconductor DS18B20 digital sensors used to measure ground temperatures around BHEs.

| | |
|---|---|
| Measurement range | from (−55) °C to +125 °C |
| Supply voltage | from 3.0 V to 5.5 V |
| Resolution | from 9 to 12 bits (0.0625 °C at 12 bit) |
| Sensor dimensions | Diameter: 6 mm<br>Length: 51 mm |
| Cover protection degree | IP65 |

The block diagram of the measurement path for measuring ground temperatures around the BHE using sensors of the DS18B20 type is shown in Figure 3.


**Figure 3.** Block diagram of the measuring path for determining ground temperatures with DS temperature sensors (based on [88]).

The tested vertical BHE probe is additionally fitted with a JS90-2.5-NE PoWoGaz flow transducer (Apator Powogaz, Toruń, Poland) with a PolluTherm microprocessor conversion system (SENSUS, Raleigh, NC, USA) and a pair of PT500 platinum thermo-resistance temperature sensors (Peak Sensors, Chesterfield, UK) mounted on the BHE supply and return connector. It allows monitoring of operating parameters in the well, such as: brine flow volume in [m$^3$], brine inlet and outlet temperature in [°C], instantaneous flow in [m$^3$/h], instantaneous power of the ground probe in [kW], and the amount of heat energy taken from the ground in [MJ]. Parameters are recorded continuously around the clock with a frequency of 300 s.

The block diagram of the measuring path for the developed test rig is shown in Figure 4.

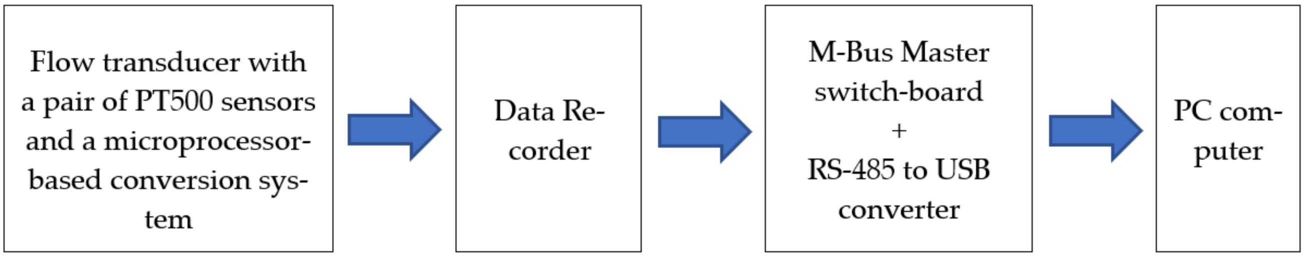


**Figure 4.** Block diagram of the measuring path for the developed test rig.

## 3. Results and Discussion

During the research, an assessment of the regeneration of one selected BHE was carried out covering the heating seasons: 2016/2017, 2017/2018, 2018/2019, 2019/2020, and the regeneration periods that follow.

The entire lower heat source for brine-water heat pumps located at the Bialystok University of Technology consists of 52 BHEs. It started working for the first time on 23 December 2014. The analysis of temperature changes in the ground covers the period from 22 September 2016 to 12 October 2020, i.e., the third, fourth, fifth, and sixth operating season of heat pumps with BHEs in a public utility building.

The paper presents the temperature distribution in the ground with an undisturbed temperature field for each month of the year (see Figure 5) to illustrate and assess the rate of changes in the ground, which was disturbed by the operation of BHEs. The time of measurement with the measuring probe covers the period from March 2015 to February 2016.

The average annual ground temperature (January–December) of the entire borehole is about 9.4 °C, and taking into account only the months of the heating season (September–April) it is about 8.7 °C, while taking into account only the summer months in the period of ground regeneration (May–August) it is 10.9 °C.

In the months (May–August), up to a depth of 5 m, the average temperature is 14.9 °C, from 5 m to 12 m it is 8.9 °C, from 12 m to 25 m it is 9.1 °C and from 25 m to 100 m it is 8.1 °C.

On the basis of Figure 5, a strong attenuation of the temperature can be seen with the change of depth. Four distinct zones of temperature changes become apparent here. The first zone, up to a depth of about 5 m, is a zone of very intense changes in soil temperature associated with the occurrence of seasons and variable temperatures of the outside air, sunlight, or precipitation. The recorded average ground temperatures vary from 1.1 °C (in January) to 22.8 °C (in August), the temperature difference is 21.7 °C. The temperatures in this layer of the ground are influenced by weather conditions. It is a zone of seasonal temperature fluctuations. Average outside air temperatures in the period March 2015–February 2016 ranged from −5.0 °C (January 2016) to 20.0 °C (August 2015) [79]. The annual insolation was 1961.9 kWh/m$^2$·year [80] and was higher than the insolation from the standard period 1991–2020, which is 1755.3 kWh/m$^2$·year (Table 2). In the second zone, at a depth of 5 m to 12 m, ground temperature changes in individual months of the year are less intense than in the first layer. The measured temperature ranges from 8.3 °C to 12.7 °C, the average temperature difference is 4.4 °C. In the third zone of the ground at a depth of 12 m to 25 m, on the basis of the tests, the recorded temperatures ranged from 8.1 °C to 9.8 °C, the temperature difference was 1.7 °C. On the other hand, in the last, fourth zone of the ground, at a depth of 25 m to 100 m, the variability of the temperature gradient is much smaller. The temperature is almost constant and rises very slowly. Figure 5 shows the temperature distribution in the ground in the studied area, in which no disturbing factors, e.g., in the form of BHEs, occurred. The geothermal heat flux for Bialystok is 0.04 W/m$^2$ [84]. On the basis of Figure 5, it can be seen that the average annual temperature in the ground (January–December) at a depth of 25 m to 100 m has a constant temperature of about 8.1 °C.

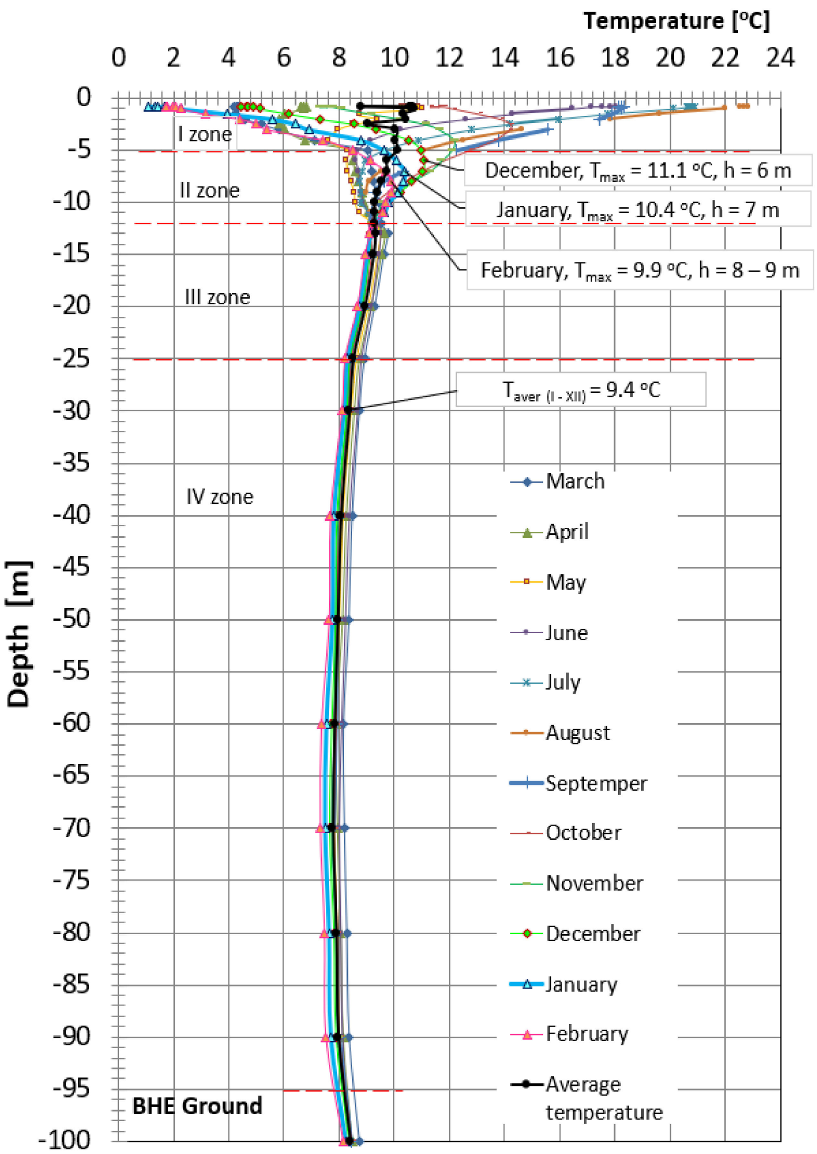


**Figure 5.** The ground temperature profile in the state of natural heat equilibrium undisturbed by BHEs in the period March 2015–February 2016.

In Poland, the heating season starts in September, and the average monthly ground temperature in September 2015 was around 11.8 °C.

During the period of the lowest temperatures of the outside air, i.e., in December, January, and February (Figure 6), it was observed that the maximum subsurface temperature of the ground occurred at depths of 6 m to 9 m (Figure 5). In December, the highest ground temperature was at a depth of 6 m and it was 11.1 °C, in January at a depth of 7 m and it was 10.4 °C, and in February at a depth of 8–9 m and it was 9.9 °C.

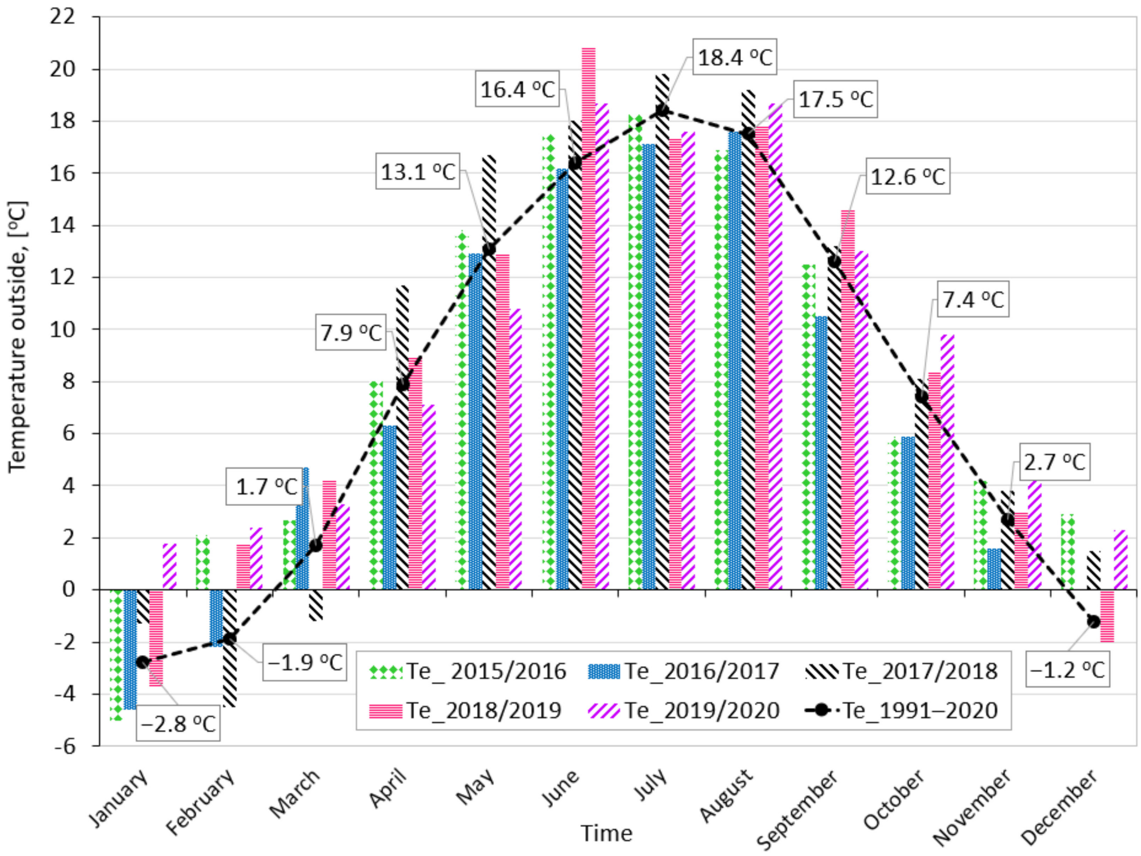


**Figure 6.** Comparison of the average annual outside air temperatures between the heating seasons in 2015–2020 with the average outside temperature based on the data for the period 1991–2020 ($T_e$—outside temperature).

In Poland, the ground temperature at a depth of 15 m to 25 m is close to the average annual air temperature [90], which was also confirmed by the research. On the basis of the measurements (Figure 5), the average annual ground temperature at a depth of 15 m to 25 m was 8.9 °C, while the average annual temperature of the outside air for Bialystok was then 8.6 °C [79].

Four heating seasons and the following periods of the ground regeneration were analyzed. The exact time of on and off switching of the brine-water heat pumps with a total heating power of 234.5 kW with BHEs in the building and the recovery time of the boreholes in the years 2016–2020 are presented in Table 6.

Particular heating seasons differed in the computational number of HDDs and outside temperatures (Figure 6), which influenced the consumption of thermal energy from the ground and its operation. A typical heating season in the measurement area lasts 232 days. On the basis of the brine-water heat pumps operation periods presented in Table 6, it can be seen that the heating seasons from 2016/2017 to 2019/2020 were shorter than the standard season and lasted from 198 days up to 205 days. It was related to warmer winters and higher average monthly temperatures than the outdoor temperatures from the years 1991–2020. In the process of interpreting the data obtained during ground regeneration, especially in the shallow zone, information on the outside air temperatures was used. The chart of annual outdoor temperatures covering heating seasons, based on data obtained from the Institute of Meteorology and Water Management [79], is shown in Figure 6.

**Table 6.** The recovery time of boreholes and operation time of brine-water heat pumps with borehole heat exchangers in the period from 22 September 2016 to 12 October 2020.

| No. | Dates | Season | The Number of Days |
|---|---|---|---|
| 1 | 22 September 2016–9 April 2017 | heat pump operation, heating season 2016/2017 | 200 |
| 2 | 10 April 2017–21 September 2017 | regeneration of wells after the heating season 2016/2017 | 165 |
| 3 | 22 September 2017–10 April 2018 | heat pump operation, heating season 2017/2018 | 201 |
| 4 | 11 April 2018–30 September 2018 | regeneration of wells after the heating season 2017/2018 | 173 |
| 5 | 1 October 2018–23 April 2019 | heat pump operation, heating season 2018/2019 | 205 |
| 6 | 24 April 2019–23 September 2019 | regeneration of wells after the heating season 2018/2019 | 153 |
| 7 | 24 September 2019–8 April 2020 | heat pump operation, heating season 2019/2020 | 198 |
| 8 | 9 April 2020–12 October 2020 | regeneration of wells after the heating season 2019/2020 | 187 |

Each start-up of heat pumps with the start of the heating season (2016/2017, 2017/2018, 2018/2019, 2019/2020) in the building of the Bialystok University of Technology resulted in a decrease in ground temperature due to the consumption of heat energy from the ground by 52 BHEs, which are the lower heat source with a design power of 184 kW.

During the extraction of heat from the ground by BHEs, the natural thermal equilibrium of the ground, shown in Figure 5, is disturbed and the temperature around the well changes. The ground temperature drops. There is a process of transient heat transfer in the ground, because both the temperature distribution around the well and the amount of heat exchanged change over time. With a properly designed and operated ground heat source and with due diligence made boreholes, the ground should regenerate every year and return to the baseline state from the previous heating season.

According to Kupiec and Larwa [91], when there is a heat exchanger in the ground and the top layer of the ground has low thermal diffusivity, the temperature profiles in the lower layers undergo significant and long-term time changes. After several years of operation of the exchanger in these conditions, the cooling of the ground may be significant, because it is not properly compensated by heat transport from the environment.

Table 4 presents the values of thermal diffusivity of individual layers in the tested well. The top layer, up to a depth of 4 m, consists of: native salt and clay ground, for which the thermal diffusivity of the layer is from $0.36{\cdot}10^{-6}$ $m^2/s$ to $0.41{\cdot}10^{-6}$ $m^2/s$.

Figure 7 shows the first analyzed heating season 2016/2017, which started on 22 September 2016. The base profile of the 2016/2017 heating season is marked in brown in the chart. Additionally, in order to compare the changes taking place in the ground, the graph shows an undisturbed profile of the ground temperatures on the same day, i.e., on 22 September 2016 measured at the control point 9.2 m away from the well (marked in black), the average temperature of which is 11.1 °C.

It can be noticed that there are temperature differences between the two profiles, the largest are up to a depth of 9 m. On average, in the entire depth up to 9 m, the temperature in the ground with an intact structure is 0.8 °C higher than the temperature of the ground, which was loaded with BHEs a year earlier (heating season 2015/2016). The biggest differences between the measured temperatures occur at a depth of 2 m to 5 m and they amount to about 1.6 °C. At a depth of 8 m to 100 m, the temperature of the ground in the borehole has a very similar profile to the ground with an undisturbed state of thermal equilibrium, the difference is only 0.1 °C.

The average annual ground temperature around the BHE before the start of the 2016/2017 heating season (22 September 2016) was 10.7 °C. The heating season lasted 200 days and ended on 9 April 2017 (the temperature profile in the ground is marked in blue). The profile shows the measured borehole temperatures on the last day of operation of the heat pumps, ending the heating season and beginning the ground regeneration period. The average temperature of the well after the end of the heating season was 2.2 °C. The blue arrow shows the direction of changes in the lowering of the temperature in the ground at particular depths during the operation of the heat pumps. Figure 7 shows the shift of the temperature profile in relation to the base profile along with examples of temperature differences between the profiles at different depths. A noticeable decrease in temperature is noticeable due to the consumption of thermal energy by the vertical ground probe. In the period of the lowest external temperatures, in the heating season at the beginning of February (8 February 2017), the average temperature in the well was also 2.2 °C.

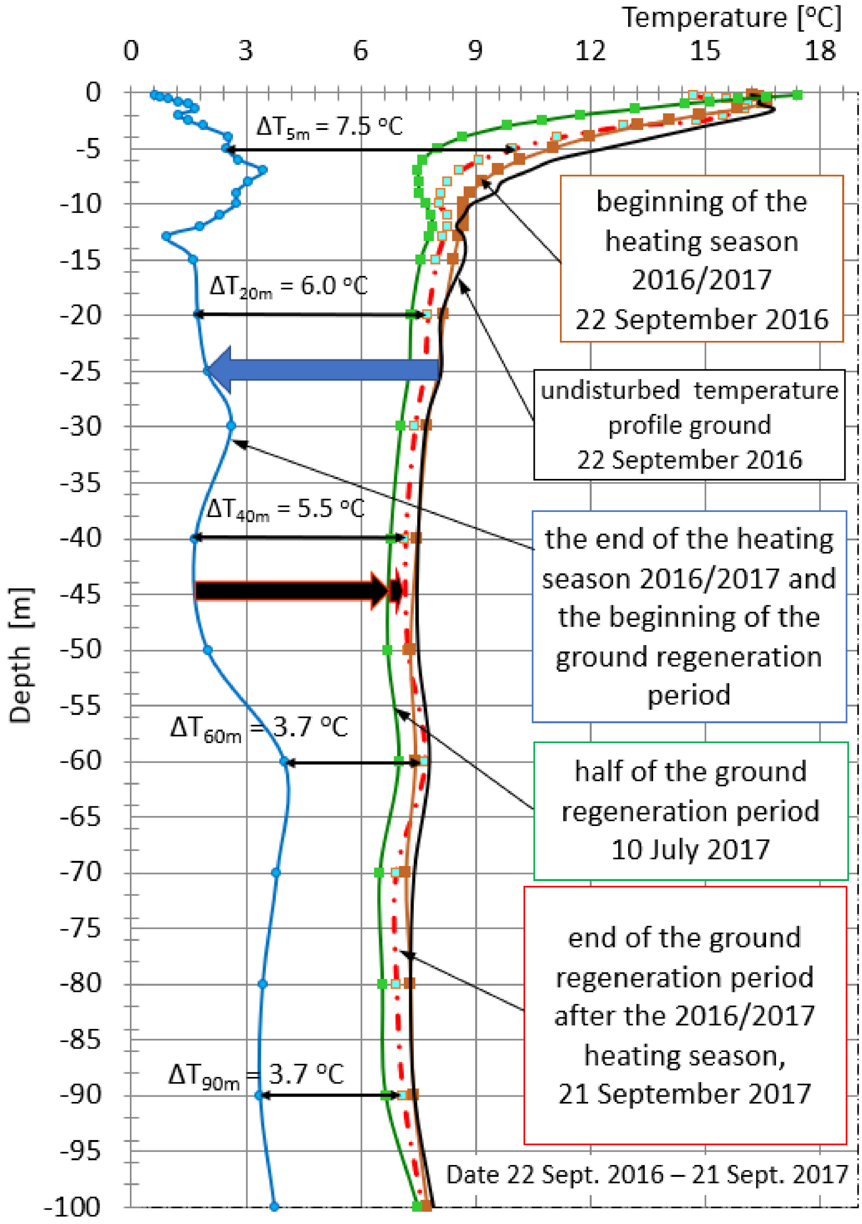


**Figure 7.** Ground temperature profiles in the well loaded with BHE work in the heating season 2016/2017 and during the ground regeneration period together with an undisturbed ground profile (of 22 September 2016). Markings: blue arrow—the direction of work of the heat source during the extraction of thermal energy from the ground, black arrow—the direction of the ground regeneration cycle.

After a 200-day heating season, the well cooled down by 8.5 °C compared to the initial temperature that started the heating season (22 September 2016). The ground regeneration period started on 10 April 2017 and lasted 165 days. The most intense changes in temperature during the regeneration period occurred in the subsurface layer, it was related to the variability of outside air temperatures (Figure 6). In the middle of the ground regeneration period (11 July 2017), the average temperature in the well was 9.3 °C, there was a rapid increase in temperature by 7.1 °C, despite the cold and rainy spring and summer period. The ground temperature distribution profile in the middle of the regeneration cycle is shown in green in Figure 7.

The process of the ground regeneration in a shallow zone from 0 to 15 m is influenced by weather conditions, and below a depth of 15–20 m, the ground temperature field is regulated by the geothermal heat of the earth and depends on the volumetric heat capacity coefficient of a given ground layer and the groundwater flow [92]. The speed of the ground regeneration process depends not only on solar radiation and increasing outside air temperature, but also on the occurrence of precipitation, which was confirmed, among others, by the ground regeneration studies after the 2016/2017 heating season.

The period of spring and the beginning of summer (April–July), when the first half of the ground regeneration falls, in 2017 (after the 2016/2017 heating season) was very rainy and humid (Appendix A). The average amount of precipitation until July was 98.4 mm with an average air humidity at that time of about 72.9%, where, in 2018 the average monthly rainfall was only 31.5 mm, and the average humidity until July was 67.4%. 2017, and thus the ground reclamation period in 2017, was very cool and very rainy compared to 2018 which was warm, dry, and sunny.

The average outside air temperature in 2017 from April to September was 13.9 °C, while in 2018 it was 16.7 °C. Nevertheless, by the middle of the ground regeneration period, the average temperature of the entire well was almost identical. After the heating season 2016/2017 it was 9.3 °C, and after the heating season 2017/2018 it was 9.2 °C (Figures 7 and 8).

Rainfall, and thus the share of flowing rainwater, influenced the regeneration of the ground most intensively to a depth of 5 m. However, the outside air temperature, for this time of the year (Table 2), was even lower than the average temperatures from the years 1991–2020. The period was also characterized by a lower intensity of solar radiation. The average monthly insolation from April to September in 2017 was 215.9 kWh/m$^2$, while in 2018 it was already 266.9 kWh/m$^2$.

The ground temperature after the completed regeneration process (21 September 2017) was 10.2 °C (red curve). Compared to the baseline profile of the well before the start of the heating season (22 September 2016), the average recorded ground temperature is 0.5 °C lower. The ground temperature profile after the regeneration period did not perfectly return to its original state, i.e., the beginning of the 2016/2017 heating season. Only at a depth of 60 m has the ground fully regenerated, this may be related to the probable occurrence of an aquifer at this depth. It is also close to the starting profile at a depth of 100 m. The aquifer in the drilling area has not been determined (Figure 1), only the hydrogeological conditions for the nearby OC1 and OC2 wells are known. And on their basis, the probability of aquifers was assumed.

The well after the completed regeneration period (21 September 2017) also did not reach temperatures identical to the profile of the ground with its intact structure. There is a measurable decrease in the temperature of the lower heat source, on average by about 0.9 °C throughout the well.

The end of the ground regeneration period 2016/2017 is also the beginning of the heating season 2017/2018.

In the following heating seasons, 2017/2018 (Figure 8), 2018/2019 (Figure 9), and 2019/2020 (Figure 10), the following assumptions were made: the beginning of a new heating season is always a profile of a regenerated well marked identically to the profile of a well from the previous season, and the end of the heating season is a blue profile, which at the same time marks the beginning of the ground regeneration period in the analyzed heating season and at the same time is the end of a given heating season.

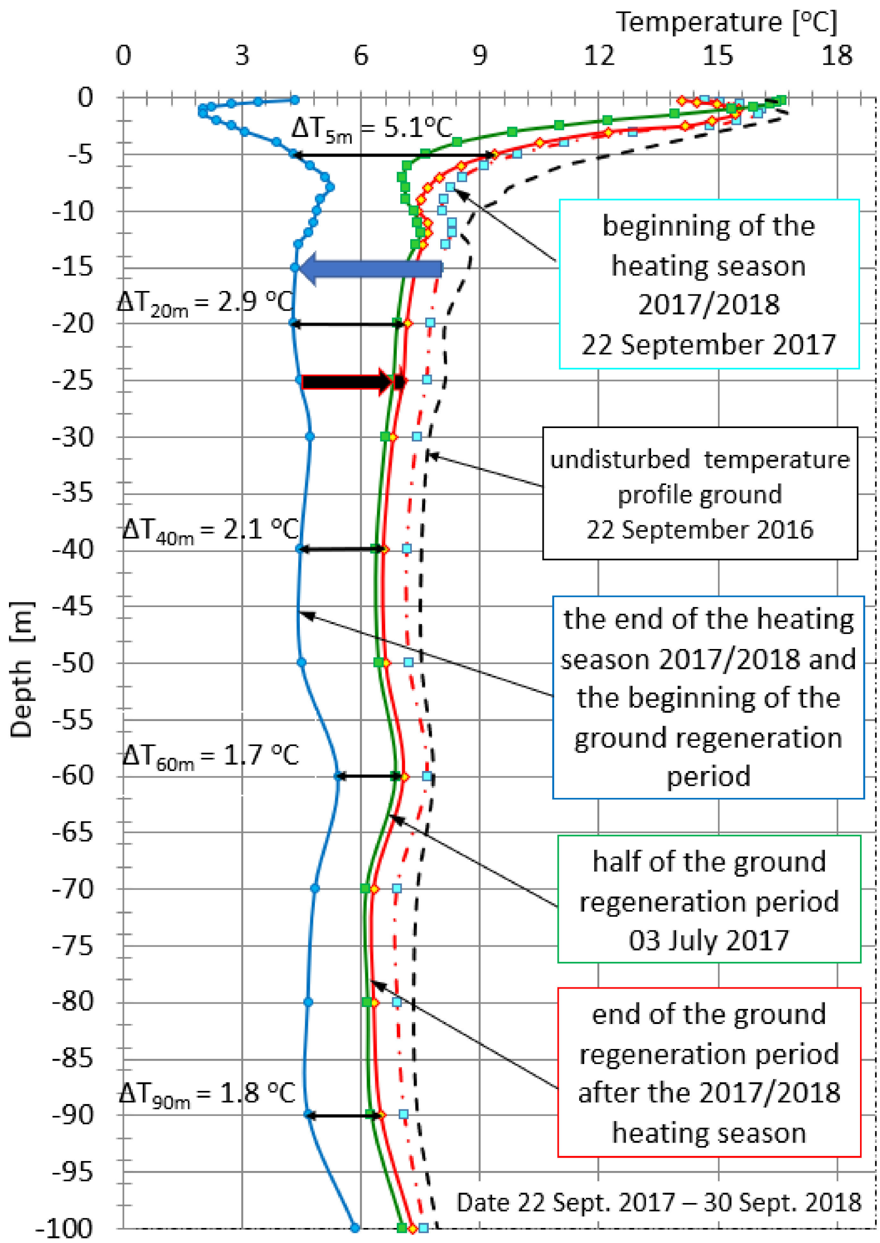


**Figure 8.** Ground temperature profiles in the well loaded with BHE work in the heating season 2017/2018 and during the ground regeneration period together with an undisturbed ground profile (of 22 September 2016). Markings: blue arrow—the direction of work of the heat source during the extraction of thermal energy from the ground, black arrow—the direction of the ground regeneration cycle.

The arrows on the charts show the direction of the processes taking place. The blue arrow shows the direction of the process of collecting thermal energy from the ground during the heating season, i.e., ground cooling, while the black arrow shows the direction and start of the ground regeneration process, i.e., ground heating and its return to the initial state of thermal equilibrium.

End of the ground regeneration process-red profile. On the other hand, the ground temperature profile marked in green shows the temperature distribution in the ground exactly in the middle of the regeneration cycle of a given heating season, which usually occurs at the beginning of July. Additionally, in Figures 8–10 the black dashed line shows the ground temperature profile in the state of undisturbed natural heat equilibrium of 22 September 2016, the beginning of the 2016/2017 heating season in order to show the changes that have occurred in the ground since then in the subsequent ones following heating seasons.

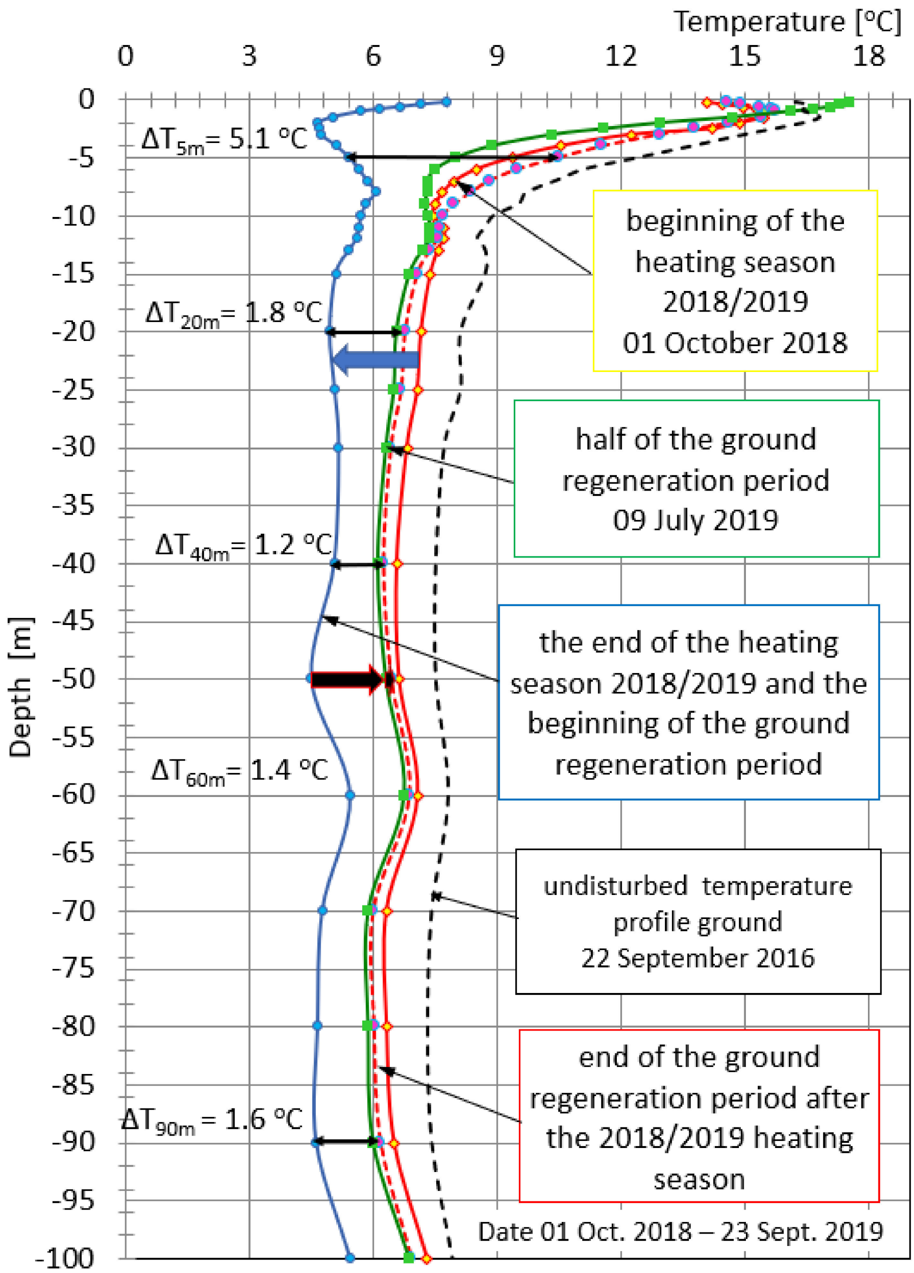


**Figure 9.** Ground temperature profiles in the well loaded with BHE work in the heating season 2018/2019 and during the ground regeneration period together with an undisturbed ground profile (of 22 September 2016). Markings: blue arrow—the direction of work of the heat source during the extraction of thermal energy from the ground, black arrow—the direction of the ground regeneration cycle.

Figure 8 shows the second analyzed heating season 2017/2018, which started on 22 September 2017. The average temperature of the well at the beginning of the starting heating season was lower by 0.5 °C compared to the 2016/2017 heating season. The base profile for this season is the temperature profile of the regenerated ground after the 2016/2017 heating season.

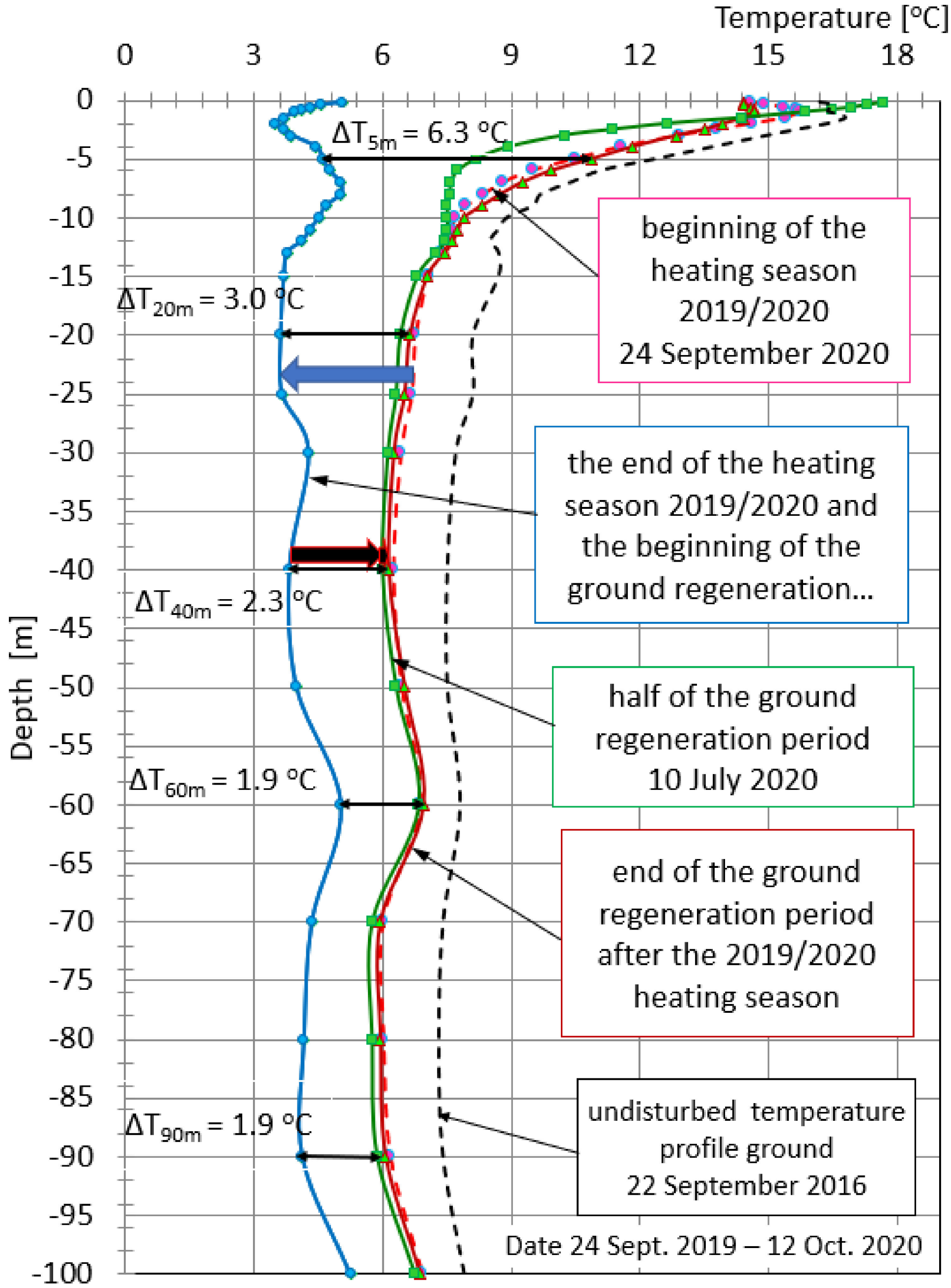


**Figure 10.** Ground temperature profiles in the well loaded with BHE work in the heating season 2019/2020 and during the ground regeneration period together with an undisturbed ground profile (of 22 September 2016). Markings: blue arrow—the direction of work of the heat source during the extraction of thermal energy from the ground, black arrow—the direction of the ground regeneration cycle.

The average temperature of the well at the beginning of the heating season was 10.2 °C, and at the end of the heating season was 4.1 °C. During the heating season, the lowest average temperature of the well was recorded at the end of February (20 February 2018) and was 1.8 °C. After the 201-day heating season, the ground cooled down by 6.1 °C, while in the 2016/2017 heating season, the ground cooled down by 8.5 °C. The differences here result from the number of HDDs in the heating season. The number of HDDs in the 2016/2017 heating season was 3276.4 day/K·year and was 102.3 day/K·year longer than in the 2017/2018 heating season. The exact duration of the season is shown in Table 6. The well's regeneration began on 11 April 2018 and lasted 173 days. In the middle of the regeneration period (86 days of regeneration), which fell on 06 July 2018, the average temperature in the well was 9.2 °C, there was a temperature increase of 5.1 °C. The temperature distribution profile in July is shown in green in Figure 8. In the second half of the ground regeneration period in 2018, the process was much slower. In the zone up to 10 m, the temperature in the ground changed on average by 1.7 °C, there the influence of weather conditions was still visible, while at depths from 10 m to 100 m the temperature change was insignificant by 0.2 °C.

The temperature in the well after the completed ground regeneration process (30 September 2018) was 9.6 °C (red curve). Compared to the well's baseline profile (22 September 2017), the average recorded ground temperature is 0.6 °C lower. After a period of ground regeneration, the well did not return perfectly to its baseline profile prior to the start of the 2017/2018 heating season. Comparing the temperature profile at the end of the ground regeneration period (30 September 2018) with the undisturbed ground profile from the 2016/2017 heating season, the temperature difference is bigger and amounts to 1.5 °C.

Figures 9 and 10 show the disturbed ground temperature profiles loaded with the BHE work for the following heating seasons: 2018/2019 and 2019/2020.

The 2018/2019 heating season started on 1 October 2018 and the average temperature of the well was 0.6 °C lower than in the 2017/2018 heating season. Figure 9 shows the third tested heating season 2018/2019. The base profile for this heating season is the temperature profile of the regenerated ground after the 2017/2018 heating season.

The average temperature of the well at the beginning of the heating season was 9.6 °C, and at the end of the heating season was 5.5 °C. During the heating season, the lowest average temperature of the well was recorded at the end of February (27 February 2019) and was 2.2 °C. After a 205-day heating season, before the beginning of the regeneration period, the temperature of the ground in the well decreased by 4.1 °C. Lower cooling of the ground in the well compared to the 2016/2017 and 2017/2018 seasons is related to the lower number of HDDs in the heating season, the amount of which depends on the outside air temperatures and the number of heating days during the year. Characteristics of heating seasons based on the number of degree days are presented in Table 3. Well regeneration began on 24-April-2019 and lasted 153 days. In the middle of the regeneration period (the 76th day of regeneration), which fell on 9 July 2019, the average temperature in the well was 9.3 °C, the temperature increased by 3.8 °C. The temperature distribution profile in July is shown in green in Figure 9. The temperature in the well after the completed ground regeneration process (23 September 2019) was 9.7 °C (red curve). Compared to the base profile of the well, the average recorded ground temperature is 0.1 °C higher, which means that the well has recovered.

The last analyzed heating season 2019/2020 started on 24 September 2019. Figure 10 shows the tested heating season 2019/2020. The base profile of this season is the temperature profile of the regenerated ground after the 2018/2019 heating season.

The average temperature of the well at the beginning of the heating season was 9.7 °C, and at the end of the heating season was 4.3 °C. After a 198-day heating season, the ground temperature in the borehole decreased by 5.4 °C. The well's regeneration started on 09 April 2020 and lasted 187 days. In the middle of the regeneration period (93 regeneration days), which fell on 10 July 2019, the average temperature in the well was 9.3 °C, since the heat pumps were turned off in the building, the temperature increased by 5.0 °C. The temperature distribution profile in July is shown in green in Figure 10. The temperature in the borehole after the completed ground regeneration process (12-October 2020) was 9.6 °C. Compared to the base profile of the well, the average recorded ground temperature is only 0.1 °C lower, which means that the well has also recovered after the 2019/2020 heating season.

Figures 8–10 show the temperature profile in the ground in the state of undisturbed natural thermal equilibrium (black line, 22 September 2016), i.e., exactly before the start of the 2016/2017 heating season. As can be seen after subsequent seasons of the ground regeneration (2017/2018—Figure 8, 2018/2019—Figure 9, 2019/2020—Figure 10), the profile was not obtained in the well as a result of self-regeneration of the ground with a profile identical or similar to the initial profile from 22 September 2016 (2016/2017). Before the start of the 2017/2018 heating season, the temperature in the well was lower by 0.9 °C (Figure 8) compared to 2016/2017. In the following year (2018/2019 season) it was lower by 1.5 °C and in the last tested season 2019/2020 lower by 1.4 °C. It follows that in the analyzed period (2016/2017–2019/2020) the tested well cooled perhaps irreversibly by about 1.4 °C.

The well cooling down without active regeneration was also achieved by Szulgowska-Zgrzywa and Fidorów-Kaprawy [93], which for three years studied the regeneration of wells in the office building. Well cooling without active regeneration averaged 0.8 °C per year. Then they simulated the operation of an actively regenerated well by injecting heat from the solar collector into the well. The simulations showed a positive effect of regeneration on the final efficiency of the tested heat pump system at the level of 3% and 4% annually in the second and third years of operation, respectively.

The process of the ground regeneration was slightly different each year (Figures 7–10), it was related to the length of the heating season and the intensity of energy consumption from the ground by BHEs. From the moment the ground regeneration process commenced, which commenced on the day the heat pumps in the building were turned off, to the end of the regeneration process (the moment when the heat pumps were turned on), the temperature increase in the borehole at different depths was not identical.

Table 7 shows the average initial temperature of the well T1 [°C] at the beginning of the ground regeneration process and the end temperature T2 [°C] at the end of the ground regeneration process during four seasons at the following depths: 5 m, 20 m, 40 m, 60 m, and 90 m (Figures 7–10) and its temperature rise. The exact date of commencement and completion of the ground regeneration is given in Table 6.

**Table 7.** Ground temperatures in the well at selected depths during the ground regeneration process (April–September) after the 2016/2017, 2017/2018, 2018/2019, and 2019/2020 heating seasons.

| Borehole Depth | The Period of the Ground Regeneration | | Temperature Rise in the Wellbore \|ΔT\| [°C] |
|---|---|---|---|
| | Initial Temperature T1 [°C] Start April | Final Temperature T2 [°C] Stop September | |
| Season 2016/2017 | | | |
| 5 m | 2.5 | 10.0 | 7.5 |
| 20 m | 1.8 | 7.8 | 6.0 |
| 40 m | 1.7 | 7.2 | 5.5 |
| 60 m | 4.0 | 7.7 | 3.7 |
| 90 m | 3.4 | 7.1 | 3.7 |
| Average | 2.2 | 10.2 | 8.0 |
| Season 2017/2018 | | | |
| 5 m | 4.3 | 9.4 | 5.1 |
| 20 m | 4.3 | 7.2 | 2.9 |
| 40 m | 4.5 | 6.6 | 2.1 |
| 60 m | 5.4 | 7.1 | 1.7 |
| 90 m | 4.7 | 6.5 | 1.8 |
| Average | 4.1 | 9.6 | 5.5 |

**Table 7.** *Cont.*

| **Borehole Depth** | **The Period of the Ground Regeneration** | | **Temperature Rise in the Wellbore \|ΔT\| [°C]** |
|---|---|---|---|
| | **Initial Temperature T1 [°C] Start April** | **Final Temperature T2 [°C] Stop September** | |
| Season 2018/2019 | | | |
| 5 m | 5.4 | 10.5 | 5.1 |
| 20 m | 5.0 | 6.8 | 1.8 |
| 40 m | 5.1 | 6.3 | 1.2 |
| 60 m | 5.5 | 6.9 | 1.4 |
| 90 m | 4.6 | 6.2 | 1.6 |
| Average | 5.5 | 9.7 | 4.2 |
| Season 2019/2020 | | | |
| 5 m | 4.6 | 10.9 | 6.3 |
| 20 m | 3.6 | 6.6 | 3.0 |
| 40 m | 3.8 | 6.1 | 2.3 |
| 60 m | 5.0 | 6.9 | 1.9 |
| 90 m | 4.2 | 6.1 | 1.9 |
| Average | 4.3 | 9.6 | 5.3 |

Based on Table 7, it can be seen that the highest temperature increases are in the subsurface zone of 5 m, while the smaller temperature increases are at greater depths, where the impact of the earth's geothermal heat flux begins. The share of geothermal heat in the total ground regeneration balance changes with depth. There is no repeatability of temperature profiles in subsequent heating seasons.

The lowest average temperature in the well starting the ground regeneration process was recorded after the 2016/2017 heating season, it was 2.2 °C (10 April), while in a similar period (9 April), but after the 2019/2020 heating season, it was 4.3 °C (Figures 7 and 10), and after the 2017/2018 heating season it was 4.1 °C (11 April), as shown in Figure 8. The highest temperature starting the regeneration of the ground around BHE was after the 2018/2019 heating season and was 5.5 °C (23 September), as shown in Figure 9.

Exactly in the middle of the ground regeneration process, despite the different lengths and temperatures of heating seasons, the average temperature in the well was similar to each other. After the 2017/2018 heating season, the average temperature of the entire well was 9.2 °C, and after the 2018/2019 and 2019/2020 heating seasons it was 9.3 °C. Despite the similar temperature in the wellbore in the subsequent heating seasons in the same period, the temperature increases differed and were not the same. The highest temperature increase was recorded after the 2016/2017 heating season and it was 7.1 °C, it was related to the well cooling down during its operation. The smallest increase was recorded after the 2018/2019 season, and it was 3.8 °C.

Based on the research, it can be noted that already halfway through the regeneration of the ground (about 77–94 days), which is most often at the beginning of July (2016/2017—01 July 2017; 2017/2018—06 July 2018; 2018/2019—09 July 2019; 2019/2020—10 July 2020), the ground regeneration phenomenon is the fastest (see Figures 8–10). In the second half of the ground regeneration period, its process is much slower, which is especially visible at depths below 10 m.

The example of research carried out in 2018 shows the rate of thermal regeneration of the ground around the BHE well in the months from April to September at selected depths in the well.

Figure 11 shows a graph of temperature changes during the course of the ground regeneration in the borehole after the 2017/2018 heating season at a depth of 1.5 m to 5 m. Figure 12 shows changes in the ground temperature at depths from 4 m to 11 m, while Figure 13 shows temperature changes at depths from 10 m to 90 m.

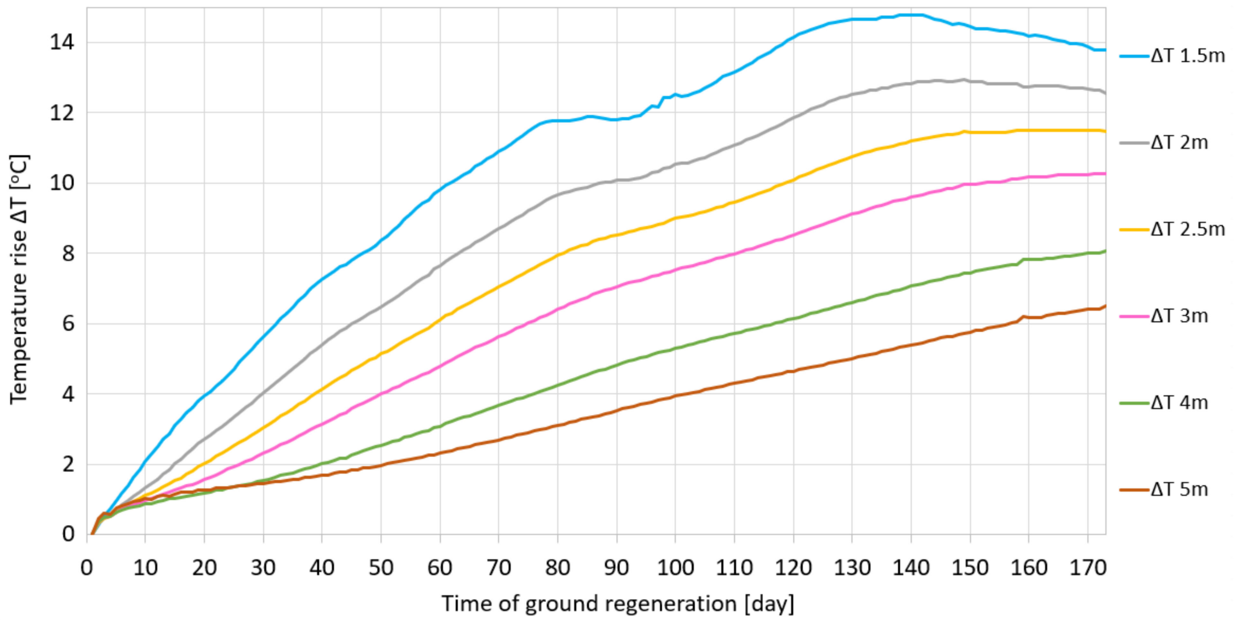


**Figure 11.** Graph of temperature changes in the tested well during the ground regeneration period (11 April 2018–30 September 2018) after the 2017/2018 heating season at depths from 1.5 m to 5 m.

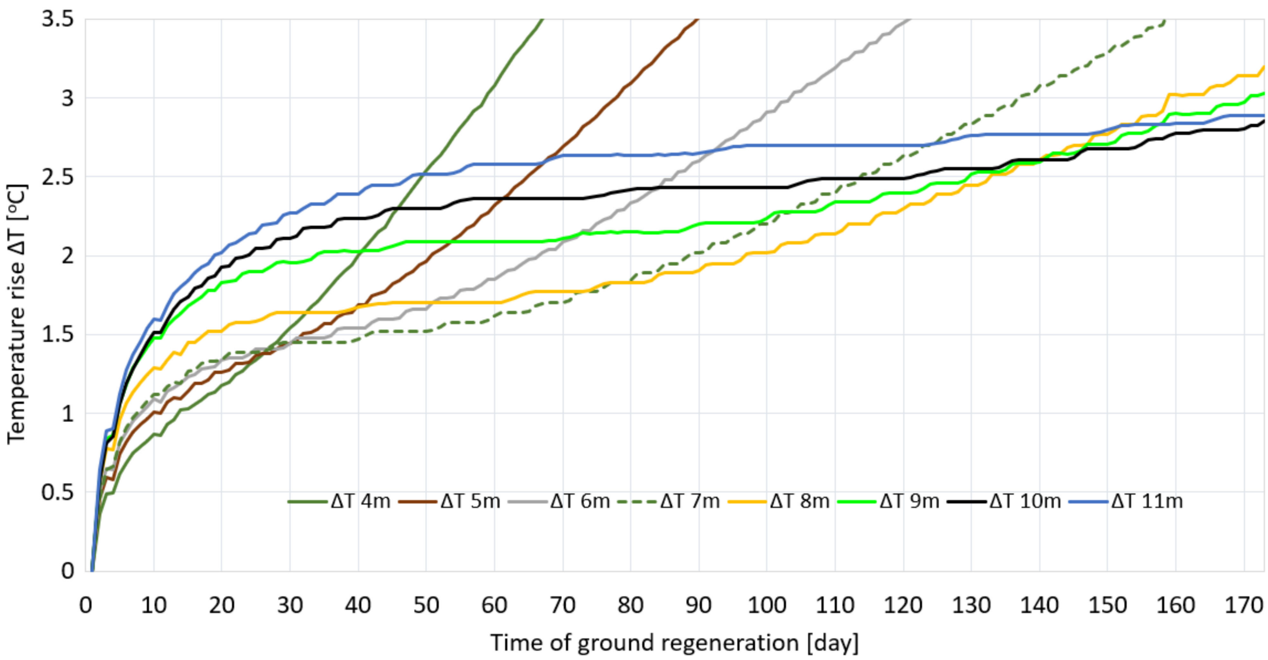


**Figure 12.** Graph of temperature changes in the tested well during the ground regeneration period (11 April 2018–30 September 2018) after the 2017/2018 heating season at depths from 4 m to 11 m.

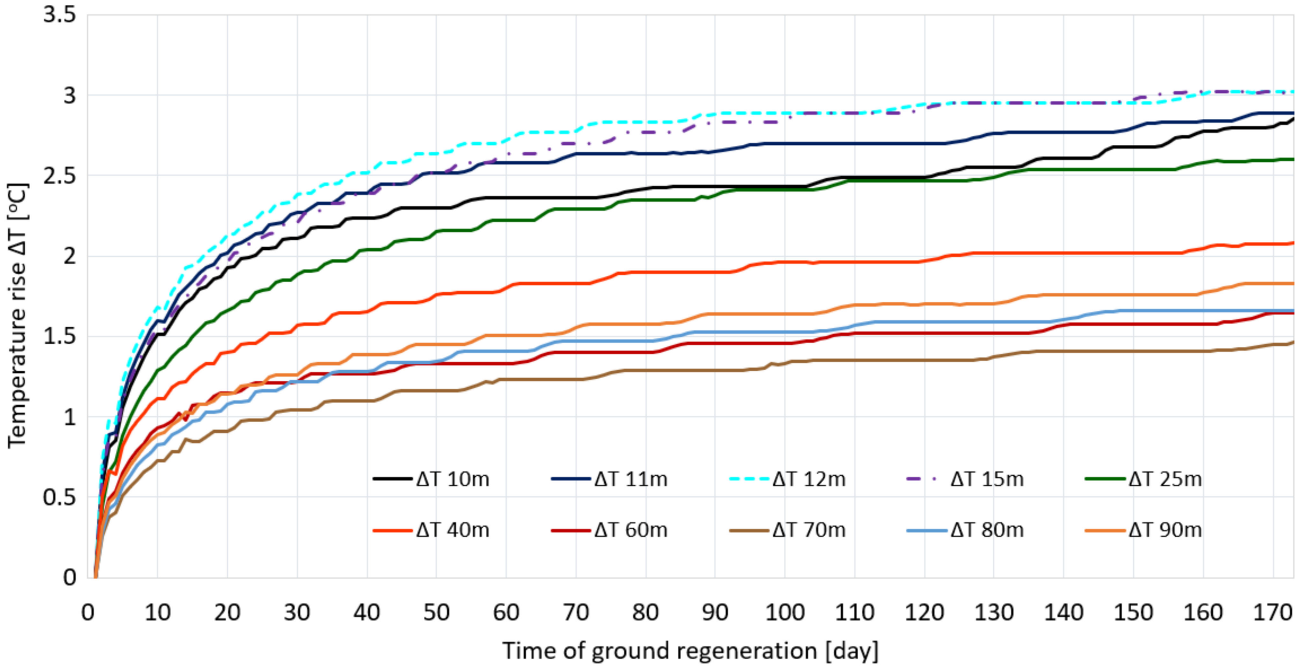


**Figure 13.** Graph of temperature changes in the tested well during the ground regeneration period (11 April 2018–30 September 2018) after the 2017/2018 heating season at depths from 10 m to 90 m.

Figure 11 shows an intense change in the ground temperature during its regeneration in layers up to 5 m, which are influenced by short-term weather conditions. The 1.5 m layer is very sensitive to the daily temperature change and reacts very quickly by heating or cooling the ground. There are noticeable fluctuations in the rise of the ground temperature. The temperature depends, among others, on rainfall, solar radiation, fluctuations in outside air temperature, or air humidity (Table 2 and Appendix A). The influence of weather conditions at different depths is marked at different times. Temperature changes at a depth of 4 m after approx. 15 days, at a depth of 5 m after approx. 25–26 days, at a depth of 6 m after approx. 33 days, at a depth of 8 m after approx. 70 days, at a depth of 9 m after approx. 85–90 days as shown in Figure 12. At a depth of 8–10 m, the impact of changes on the surface is insignificant compared to the shallower layers. The regeneration process showed the influence of weather conditions at a depth of 10 m after about 110 days and a very insignificant effect at a depth of 12 m (Figure 13). At a depth of 15 m in the borehole, the influence of weather conditions is imperceptible, as well as at depths from 25 m to 90 m. In this case, the ground temperature is almost constant, it rises very slowly due to the thermal influence of the earth's interior.

Figure 14 shows the distribution of soil temperatures at different depths in a 100 m well bore on 01 September 2015, 01 September 2016, 01 September 2018, 01 September 2019 and 01 September 2020. The temperature in the wellbore was measured on the same day over the course of several years and, as it can be seen in the chart, it was not the same. Temperature drop is noticeable here. During the first year of soil regeneration on 01 September 2015, the average temperature in the well was 11.8 °C, the remaining average temperatures measured on 01 September in 2016–2020 are presented in Table 8.

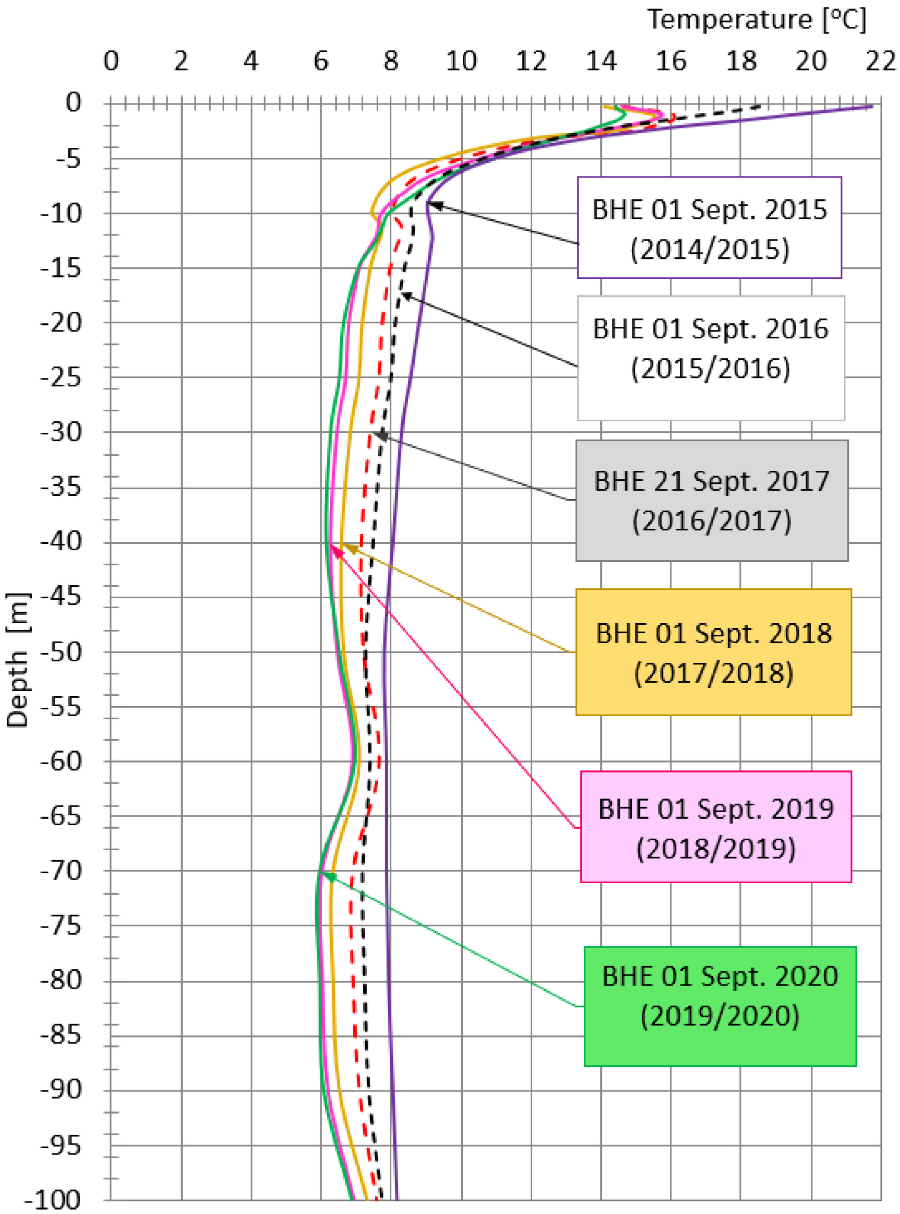


**Figure 14.** Ground temperature profiles with BHE during the ongoing period of ground self-regeneration on September 1 recorded in years 2015–2020.

**Table 8.** The average temperature in the well on the selected date in the years 2015–2020.

| No. | Dates | Average Well Temperature [°C] |
|---|---|---|
| 1 | 1 September 2015 | 11.8 |
| 2 | 1 September 2016 | 10.7 |
| 3 | 1 September 2017<br>21 September 2017 | *<br>10.2 |
| 4 | 1 September 2018 | 9.6 |
| 5 | 1 September 2019 | 9.7 |
| 6 | 1 September 2020 | 9.6 |

*—no data registration 1 September 2017.

None of the ground temperature profiles in the well in the four analyzed heating seasons reached the temperatures in September recorded in the ground on 1 September 2015. The temperature difference between 1 September 2015 and 1 September 2020 is 2.2 °C.

The average well temperature, recorded on the 1st of September, reflects the temperature of the recovered ground at the end of the well regeneration period. The well regeneration process, as shown in Figures 11–13 in September (145 recovery days), is already very slow at depths from 10 m due to the decreasing temperature gradients.

In 2018–2020, the average temperature in the well, both measured on the 1st of September and at the end of the ground regeneration period after the 2017/2018, 2018/2019 and 2019/2020 seasons, remains at almost the same level, amounting to 9.6–9.7 °C. After four years of operation, the temperature in the well decreased by 2.2 °C, the fifth and the sixth year of operation did not bring any further changes in the ground temperature reduction (Table 8). Perhaps it is a new thermal equilibrium between BHE and the ground. However, only the ground research and its observations in the coming years will be able to confirm this thesis.

A similar phenomenon was noticed and described by Rybach and Sanner [92]. They found that in the near field around the heat exchanger, the ground cools down during the first 2–3 years of operation. The temperature deficit decreases from year to year until a new stable thermal equilibrium is established between the BHE and the ground, at temperatures about 1–2 °C lower than originally. Despite the cooling of the ground, there is no sudden drop in the efficiency of the heat source. In any case, this can be understood as pure coincidence, but as you can see, similar cases are already known. Therefore, it should be taken into account that if the initial thermal conditions do not improve between seasons in any facility, it is due to the net amount of energy exchange, the configuration of the BHE field, and the local geological and hydrogeological conditions. The above-mentioned authors also simulated the operation of the BHE over a 30-year period and the recovery of heat from the ground over a period of 25 years after its end-of-life. The obtained results confirmed that the temperature near BHE in winter drops quickly in the first years and remains more or less stable in the following years. In summer, the initial temperatures are not reached again, but the temperature drop decreases from year to year. After the end of the operation, quick heat recovery can be observed after the heating season, followed by a slowdown of this process due to decreasing temperature gradients [84].

## 4. Conclusions

Based on the conducted research, the phenomenon of thermal ground regeneration in the period between the heating seasons 2016/2017, 2017/2018, 2018/2019, and 2019/2020 was verified on the basis of the recorded data. The GSHP installation during the heating season works exclusively for heating purposes of the building. The obtained results show that in successive heating seasons there is no repeatability of temperature distribution in the ground, both during the heating season and the course of the ground regeneration process. Additionally:

- In the layer at a depth of 6–9 m, in the coldest months in Poland, from December to February, the occurrence of maximum temperatures at the level of 9.9 °C (February)–11.1 °C (December), where the average annual ground temperature at a depth of 25 m to 100 m is 8.1 °C. Perhaps it would be reasonable and economical to use, when designing lower heat sources, to a much greater extent these ground layers, e.g., by drilling oblique boreholes, basket heat exchangers, and others.
- The measurements confirmed that at a depth of 15–25 m, the average annual ground temperature has a temperature close to the annual average outside air temperature, and in shallow, near-surface zones, the ground temperature changes seasonally under the influence of weather conditions, that are difficult to predict [91,94–97].
- Despite shorter heating seasons lasting 200–201 days and the number of HDDs in the heating season 3174.1–3276.4 days/K year, in 2016–2018, compared to the standard

season, which lasts 232 days, where the number of HDDs is 3496.1 day/K year, the well under test has not fully recovered. However, in the 2018/2019 and 2019/2020 seasons, the ground temperature during regeneration returned to the baseline from before the preceding heating season.

Despite the full regeneration of the ground in the last two heating seasons, in the studied period from 22 September 2016 to 12 October 2020, the ground probably cooled irreversibly by 1.5 °C. However, taking into account the years 2015–2020, the cooling of the ground is already 2.2 °C. The average annual temperature of the well in 2015 was 11.8 °C, and in 2020 it is 9.6 °C.

- With such long heating seasons (in cold regions), it seems reasonable to use an additional heat source at the stage of designing ground heat exchangers, supporting ground regeneration in the summer. Ground regeneration in summer can be supported by, among others, PV panels with electric heaters or liquid solar collectors, which in the case of public buildings, especially schools, would allow the use of excess thermal energy obtained from solar collectors, mainly during the holiday season, which is a huge problem, especially in schools, in the months of VII–VIII.
- It also seems justified due to the intensity of solar radiation in the summer, and thus the amount of heat that cannot be quickly pumped into the ground in order to regenerate BHE, the use of underground energy storage, because in a cold climate without adequate heat injection in summer, the ground temperature may not return to its natural state, and this process may worsen with each passing year. The use of underground energy storage or hybrid systems will help to reduce the carbon footprint, which is one of the main goals of the European Green Deal.
- The weather conditions affect the ground regeneration process in the zone from 0–12 m. At the same time, the influence of weather conditions at different depths is not marked simultaneously at the same time. The reaction time depends on the depth, the deeper it is, the longer it is, e.g., in the zone at a depth of 4 m, it started after about 15 days, but at a depth of 10 m after about 110 days. A slight influence was observed at a depth of 12 m, and was imperceptible at depths of 15–100 m. Rybach and Sanner [92] showed that the zone of the influence of atmospheric conditions in the place of their research was 0–15 m.
- The process of ground regeneration is most intensive until the middle of its time (it is usually the beginning of July), then its further regeneration is very slow, especially at depths below 10 m, the influence of climatic conditions is less noticeable here. Below the depth of 12 m, the ground temperature field is regulated by the geothermal heat flux from the interior of the Earth and the possible flow of groundwater.
- The average temperature of the regenerated ground in 2018–2020 (the fifth and sixth heating season) remains at the same level of 9.6–9.7 °C, hence it is possible that a new stable thermal equilibrium has been established between the BHE and the ground. Possibly, it may be related, in this period, to warmer winters and a shorter heating season, and thus a longer period of the ground regeneration around the BHE. However, only further research, which the author will provide in the following years, will allow to confirm, or reject this thesis.
- The conducted research will help to better understand the changes taking place in the ground, and thus to better design lower heat sources for heat pumps systems, whether in the form of horizontal, vertical, oblique, or basket ground heat exchangers. They can be used to validate numerical models for convection and conduction of heat transport in the ground. The obtained results of measurements of temperature in the ground can be used for long-term simulations and are very valuable information, allowing for the introduction of, for example, corrections in very ideal, sometimes theoretical mathematical models, used to simulate lower heat sources, and allow to see the complexity of processes related to heat and mass transfer occurring in the ground.

- The article contributes to the scientific community, particularly by showing a very relevant and useful technical approach to quantify the cooling effect of soil based on detailed long-term monitoring of ground temperatures.
- From the point of view of the proper exploitation of the ground heat source, it seems important to introduce monitoring of shallow geothermal systems, especially in the case of large and extensive BHE installations. The number of checkpoints should depend on the number of GHE or installed thermal power. The ground monitoring should also be accompanied by the control of all other important technical parameters of the GSHP room, such as electricity consumption, inlet, and outlet temperatures of the evaporator and GSHP condenser, compressor operating hours, etc.

**Funding:** The research was carried out as part of the work No. (WZ/WBiIS/4/2020) at the Bialystok University of Technology and financed from a research subsidy provided by the Minister of Education and Science of the Republic of Poland, co-funded by the European Union through the European Regional Development Fund under the Programme Infrastructure and Environment.

**Institutional Review Board Statement:** Not applicable.

**Informed Consent Statement:** Not applicable.

**Data Availability Statement:** Not applicable.

**Acknowledgments:** Meteorological data are available thanks to the kindness of the Institute of Meteorology and Water Management—National Research Institute (IMGW-PIB). Maps are available thanks to the kindness of the Polish Geological Institute and European Union (https://europa.eu/european-union/about-eu/easy-to-read_en; accessed on 28 July 2021).

**Conflicts of Interest:** The authors declare no conflict of interest.

## Appendix A

In order to thoroughly analyze the temperature changes occurring in the upper layers around the well, during its regeneration, Table A1 presents the average insolation, average daily humidity and average rainfall for the years 2016–2020 and the multi-year period 1991–2020 for the analyzed area.

Average insolation, humidity and total precipitation for the area covered by the research on the regeneration phenomenon (Data from the Institute of Meteorology and Water Management) [79].

**Table A1.** The average insolation, average daily humidity and average rainfall for the years 2016–2020 and the multi-year period 1991–2020 for the analyzed area.

| Month | Insolation [kWh/m$^2$] | | | | | |
|---|---|---|---|---|---|---|
| | Statistical 1991–2020 | 2016 (2015/2016) * | 2017 (2016/2017) * | 2018 (2017/2018) * | 2019 (2018/2019) * | 2020 (2019/2020) * |
| IV | 185.7 | 142.8 | 169.7 | 248.6 | 292.6 | 255.7 |
| V | 254.1 | 295.7 | 279.9 | 363.2 | 195.0 | 227.2 |
| VI | 259.3 | 313.0 | 237.7 | 259.9 | 371.9 | 245.0 |
| VII | 256.9 | 177.1 | 252.5 | 202.0 | 257.6 | 261.4 |
| VIII | 250.5 | 216.1 | 237.7 | 294.3 | 298.4 | 258.0 |
| IX | 161.8 | 202.6 | 117.7 | 233.5 | 203.3 | 225.9 |
| Average | 233.0 | 224.6 | 215.9 | 266.9 | 269.8 | 245.5 |
| Annually I-XII | 1755.3 | 1688.9 | 1553.9 | 2008.5 | 2032.2 | 1846.1 |
| Month | Humidity [%] | | | | | |
| | Statistical 1991–2020 | 2016 (2015/2016) * | 2017 (2016/2017) * | 2018 (2017/2018) * | 2019 (2018/2019) * | 2020 (2019/2020) * |
| IV | 69.8 | 67.9 | 73.0 | 68.0 | 54.4 | 55.8 |
| V | 71.2 | 69.7 | 67.4 | 63.7 | 73.6 | 69.0 |
| VI | 73.1 | 68.3 | 73.4 | 62.3 | 67.9 | 75.9 |
| VII | 75.4 | 79.7 | 77.7 | 77.2 | 73.8 | 73.8 |
| VIII | 77.2 | 80.5 | 79.6 | 74.9 | 78.6 | 75.0 |
| IX | 82.5 | 80.9 | 85.4 | 78.6 | 79.2 | 81.5 |
| Average | 74.9 | 74.5 | 76.1 | 70.8 | 71.3 | 71.8 |
| Annually I–XII | 80.5 | 79.9 | 81.4 | 78.0 | 77.9 | 79.0 |
| Month | Total Precipitation [mm] | | | | | |
| | Statistical 1991–2020 | 2016 (2015/2016) * | 2017 (2016/2017) * | 2018 (2017/2018) * | 2019 (2018/2019) * | 2020 (2019/2020) * |
| IV | 37.7 | 37.3 | 78.0 | 41.0 | 4.1 | 5.1 |
| V | 69.1 | 46.7 | 101.1 | 31.2 | 100.4 | 72.0 |
| VI | 65.4 | 44.4 | 116.1 | 22.4 | 50.3 | 138.6 |
| VII | 86.5 | 186.6 | 82.8 | 144.8 | 113.5 | 43.2 |
| VIII | 69.4 | 68.6 | 108.2 | 25.9 | 100.7 | 97.5 |
| IX | 56.0 | 21.5 | 123.4 | 65.9 | 54.0 | 24.5 |
| Average | 64.0 | 67.5 | 101.6 | 55.2 | 70.5 | 63.5 |
| Annually I–XII | 610.2 | 790.0 | 934.6 | 536.2 | 617.6 | 639.9 |

*—heating season.

## References

1. European Parliament. European Parliament Resolution of 15 January 2020 on the European Green Deal 2019, 2956 (RSP). Available online: https://www.europarl.europa.eu/doceo/document/TA-9-2020-0005_EN.html (accessed on 10 June 2021).
2. European Parliament. European Parliament Resolution of 14 March 2019 on Climate Change-A European Strategic Long-Term Vision for a Prosperous, Modern, Competitive and Climate Neutral Economy in Accordance with the Paris Agreement 2019, 2582(RSP). Available online: https://www.europarl.europa.eu/doceo/document/TA-8-2019-0217_EN.html (accessed on 9 June 2021).
3. International Energy Agency (IEA). *Global Status Report for Buildings and Construction 2019*; IEA: Paris, France, 2019; Available online: https://www.iea.org/reports/global-status-report-for-buildings-and-construction (accessed on 9 June 2021).

4. United Nations Environment Programme. *2020 Global Status Report for Buildings and Construction: Towards a Zero-Emission, Efficient and Resilient Buildings and Construction Sector*; United Nations Environment Programme: Nairobi, Kenya, 2020; Available online: https://globalabc.org/news/launched-2020-global-status-report-buildings-and-construction (accessed on 5 June 2021).
5. Zhao, Y.; Pang, Z.; Huang, Y.; Ma, Z. An efficient hybrid model for thermal analysis of deep borehole heat exchangers. *Geotherm. Energy* **2020**, *8*, 18. [CrossRef]
6. Zarrella, A.; Emmi, G.; Graci, S.; De Carli, M.; Cultrera, M.; Santa, G.D.; Galgaro, A.; Bertermann, D.; Müller, J.; Pockelé, L.; et al. Thermal Response Testing Results of Different Types of Borehole Heat Exchangers: An Analysis and Comparison of Interpretation Methods. *Energies* **2017**, *10*, 801. [CrossRef]
7. Lee, S.-M.; Park, S.-H.; Jang, Y.-S.; Kim, E.-J. Proposition of Design Capacity of Borehole Heat Exchangers for Use in the Schematic-Design Stage. *Energies* **2021**, *14*, 822. [CrossRef]
8. Minaei, A.; Maerefat, M. A new analytical model for short-term borehole heat exchanger based on thermal resistance capacity model. *Energy Build.* **2017**, *146*, 233–242. [CrossRef]
9. Boban, L.; Miše, D.; Herceg, S.; Soldo, V. Application and Design Aspects of Ground Heat Exchangers. *Energies* **2021**, *14*, 2134. [CrossRef]
10. Naicker, S.S.; Rees, S.J. Long-term high frequency monitoring of a large borehole heat exchanger array. *Renew. Energy* **2020**, *145*, 1528–1542. [CrossRef]
11. Spitler, J.; Bernier, M. 2-Vertical borehole ground heat exchanger design methods. In *Advances in Ground-Source Heat Pump Systems*; Rees, S.J., Ed.; Woodhead Publishing: Oxford, UK, 2016; pp. 29–61. ISBN 978-0-08-100311-4. [CrossRef]
12. Kasuda, T.; Archenbach, P. *Earth Temperature and Thermal Diffusivity at Selected Stations in the United States*; National Bureau of Standards: Gaithersburg, MD, USA, 1965. [CrossRef]
13. Nian, Y.; Cheng, W. Analytical g-function for vertical geothermal boreholes with effect of borehole heat capacity. *Appl. Therm. Eng.* **2018**, *140*, 733–744. [CrossRef]
14. Yu, X.; Li, H.; Yao, S.; Nielsen, V.; Heller, A. Development of an efficient numerical model and analysis of heat transfer performance for borehole heat exchanger. *Renew. Energy* **2020**, *152*, 189–197. [CrossRef]
15. Wang, C.; Li, H.; Huang, Z.; Lu, Y.; Huang, X.; Gan, L. A new heat transfer model for single U-pipe ground heat exchanger. *Appl. Therm. Eng.* **2019**, *154*, 400–406. [CrossRef]
16. Ghoreish-Madiseh, S.; Kuyuk, A.; de Brito, M.A.R. An analytical model for transient heat transfer in ground-coupled heat exchangers of closed-loop geothermal systems. *Appl. Therm. Eng.* **2019**, *150*, 696–705. [CrossRef]
17. Li, P.; Guan, P.; Zheng, J.; Dou, B.; Tian, H.; Duan, X.; Liu, H. Field Test and Numerical Simulation on Heat Transfer Performance of Coaxial Borehole Heat Exchanger. *Energies* **2020**, *13*, 5471. [CrossRef]
18. Zhou, A.; Huang, X.; Wang, W.; Jiang, P.; Li, X. Thermo-Hydraulic Performance of U-Tube Borehole Heat Exchanger with Different Cross-Sections. *Sustainability* **2021**, *13*, 3255. [CrossRef]
19. Javadi, H.; Urchueguia, J.F.; Mousavi Ajarostaghi, S.S.; Badenes, B. Numerical Study on the Thermal Performance of a Single U-Tube Borehole Heat Exchanger Using Nano-Enhanced Phase Change Materials. *Energies* **2020**, *13*, 5156. [CrossRef]
20. Katsura, T.; Sakata, Y.; Ding, L.; Nagano, K. Development of Simulation Tool for Ground Source Heat Pump Systems Influenced by Ground Surface. *Energies* **2020**, *13*, 4491. [CrossRef]
21. Mitchell, M.S.; Spitler, J.D. An Enhanced Vertical Ground Heat Exchanger Model for Whole-Building Energy Simulation. *Energies* **2020**, *13*, 4058. [CrossRef]
22. Jahanbin, A.; Semprini, G.; Natale Impiombato, A.; Biserni, C.; Rossi di Schio, E. Effects of the Circuit Arrangement on the Thermal Performance of Double U-Tube Ground Heat Exchangers. *Energies* **2020**, *13*, 3275. [CrossRef]
23. Hałaj, E.; Pająk, L.; Papiernik, B. Finite Element Modeling of Geothermal Source of Heat Pump in Long-Term Operation. *Energies* **2020**, *13*, 1341. [CrossRef]
24. Katsura, T.; Higashitani, T.; Fang, Y.; Sakata, Y.; Nagano, K.; Akai, H.; Oe, M. A New Simulation Model for Vertical Spiral Ground Heat Exchangers Combining Cylindrical Source Model and Capacity Resistance Model. *Energies* **2020**, *13*, 1339. [CrossRef]
25. Zhang, X.; Zhang, T.; Li, B.; Jiang, Y. Comparison of Four Methods for Borehole Heat Exchanger Sizing Subject to Thermal Response Test Parameter Estimation. *Energies* **2019**, *12*, 4067. [CrossRef]
26. Naldi, C.; Zanchini, E. Full-Time-Scale Fluid-to-Ground Thermal Response of a Borefield with Uniform Fluid Temperature. *Energies* **2019**, *12*, 3750. [CrossRef]
27. Quaggiotto, D.; Zarrella, A.; Emmi, G.; De Carli, M.; Pockelé, L.; Vercruysse, J.; Psyk, M.; Righini, D.; Galgaro, A.; Mendrinos, D.; et al. Simulation-Based Comparison Between the Thermal Behavior of Coaxial and Double U-Tube Borehole Heat Exchangers. *Energies* **2019**, *12*, 2321. [CrossRef]
28. Rivoire, M.; Casasso, A.; Piga, B.; Sethi, R. Assessment of Energetic, Economic and Environmental Performance of Ground-Coupled Heat Pumps. *Energies* **2018**, *11*, 1941. [CrossRef]
29. Sun, X.-H.; Yan, H.; Massoudi, M.; Chen, Z.-H.; Wu, W.-T. Numerical Simulation of Nanofluid Suspensions in a Geothermal Heat Exchanger. *Energies* **2018**, *11*, 919. [CrossRef]
30. Alberti, L.; Angelotti, A.; Antelmi, M.; La Licata, I.A. Numerical Study on the Impact of Grouting Material on Borehole Heat Exchangers Performance in Aquifers. *Energies* **2017**, *10*, 703. [CrossRef]
31. Puttige, A.R.; Andersson, S.; Östin, R.; Olofsson, T.A. Novel Analytical-ANN Hybrid Model for Borehole Heat Exchanger. *Energies* **2020**, *13*, 6213. [CrossRef]

32. Lei, X.; Zheng, X.; Duan, C.; Ye, J.; Liu, K. Three-Dimensional Numerical Simulation of Geothermal Field of Buried Pipe Group Coupled with Heat and Permeable Groundwater. *Energies* **2019**, *12*, 3698. [CrossRef]
33. Sáez Blázquez, C.; Farfán Martín, A.; Martín Nieto, I.; Carrasco García, P.; Sánchez Pérez, L.S.; González-Aguilera, D. Efficiency Analysis of the Main Components of a Vertical Closed-Loop System in a Borehole Heat Exchanger. *Energies* **2017**, *10*, 201. [CrossRef]
34. Neuberger, P.; Adamovský, R. Analysis and Comparison of Some Low-Temperature Heat Sources for Heat Pumps. *Energies* **2019**, *12*, 1853. [CrossRef]
35. Rad, F.M.; Fung, A.S.; Rosen, M.A. An integrated model for designing a solar community heating system with borehole thermal storage. *Energy Sustain. Dev.* **2017**, *36*, 6–15. [CrossRef]
36. Viccaro, M. Doped bentonitic grouts for implementing performances of low-enthalpy geothermal systems. *Geotherm. Energy* **2018**, *6*, 4. [CrossRef]
37. Ouzzane, M.; Eslami-Nejad, P.; Aidoun, Z.; Lamarche, L. Analysis of the convective heat exchange effect on the undisturbed ground temperature. *Sol. Energy* **2014**, *108*, 340–347. [CrossRef]
38. Pan, A.; Lu, L.; Tian, Y. A new analytical model for short vertical ground heat exchangers with Neumann and Robin boundary conditions on ground surface. *Int. J. Therm. Sci.* **2020**, *152*, 106–326. [CrossRef]
39. Nian, Y.; Wang, X.; Xie, K.; Cheng, W. Estimation of ground thermal properties for coaxial BHE through distributed thermal response test. *Renew. Energy* **2020**, *152*, 1209–1219. [CrossRef]
40. Boban, L.; Soldo, V.; Fuji, H. Investigation of heat pump performance in heterogeneous ground. *Energy Convers. Manag.* **2020**, *211*, 112–736. [CrossRef]
41. Ahmadfard, M.; Bernier, M. A review of vertical ground heat exchanger sizing tools including an intermodel comparison. Renew. *Sustain. Energy Rev.* **2019**, *110*, 247–265. [CrossRef]
42. Sailer, E.; Taborda, D.M.G.; Zdravković, L. A new approach to estimating temperature fields around a group of vertical ground heat exchangers in two-dimensional analyses. *Renew. Energy* **2018**, *118*, 579–590. [CrossRef]
43. Hu, J. An improved analytical model for vertical borehole ground heat exchanger with multiple-layer substrates and groundwater flow. *Appl. Energy* **2017**, *202*, 537–549. [CrossRef]
44. Morchio, S.; Fossa, M. On the ground thermal conductivity estimation with coaxial borehole heat exchangers according to different undisturbed ground temperature profiles. *Appl. Therm. Eng.* **2020**, *173*, 115–198. [CrossRef]
45. Beier, R.A. Thermal response tests on deep borehole heat exchangers with geothermal gradien. *Appl. Therm. Eng.* **2020**, *178*, 115–447. [CrossRef]
46. Gónzález-Santander, J.L. Asymptotic expansions for the ground heat transfer due to a borehole heat exchanger with a Neumann boundary condition. *J. Eng. Math.* **2019**, *117*, 47–64. [CrossRef]
47. Kerme, E.D.; Fung, A.S. Heat transfer simulation, analysis and performance study of single U-tube borehole heat exchanger. *Renew. Energy* **2020**, *145*, 1430–1448. [CrossRef]
48. Claesson, J.; Javed, S. Explicit Multipole Formulas for Calculating Thermal Resistance of Single U-Tube Ground Heat Exchangers. *Energies* **2018**, *11*, 214. [CrossRef]
49. Naldi, C.; Jahanbin, A.; Zanchini, E. A New Estimate of Sand and Grout Thermal Properties in the Sandbox Experiment for Accurate Validations of Borehole Simulation Codes. *Energies* **2021**, *14*, 1149. [CrossRef]
50. Sivasakthivel, T.; Philippe, M.; Murugesan, K.; Verma, V.; Hu, P. Experimental thermal performance analysis of ground heat exchangers for space heating and cooling applications. *Renew. Energy* **2017**, *113*, 1168–1181. [CrossRef]
51. Zhai, X.; Cheng, X.; Wang, R. Heating and cooling performance of a mini type ground source heat pump system. *Appl. Therm. Eng.* **2017**, *111*, 1366–1370. [CrossRef]
52. Atwany, H.; Hamdan, M.O.; Abu-Nabah, B.A.; Alami, A.H.; Attom, M. Experimental evaluation of ground heat exchanger in UAE. *Renew. Energy* **2020**, *159*, 538–546. [CrossRef]
53. Vella, C.; Borg, S.P.; Micallef, D. The Effect of Shank-Space on the Thermal Performance of Shallow Vertical U-Tube Ground Heat Exchangers. *Energies* **2020**, *13*, 602. [CrossRef]
54. Zarrella, A.; Zecchin, R.; Pasquier, P.; Guzzon, D.; Prataviera, E.; Vivian, J.; De Carli, M.; Emmi, G. Analysis of Retrofit Solutions of a Ground Source Heat Pump System: An Italian Case Study. *Energies* **2020**, *13*, 5680. [CrossRef]
55. Bartolini, N.; Casasso, A.; Bianco, C.; Sethi, R. Environmental and Economic Impact of the Antifreeze Agents in Geothermal Heat Exchangers. *Energies* **2020**, *13*, 5653. [CrossRef]
56. Badenes, B.; Mateo Pla, M.Á.; Magraner, T.; Soriano, J.; Urchueguía, J.F. Theoretical and Experimental Cost–Benefit Assessment of Borehole Heat Exchangers (BHEs) According to Working Fluid Flow Rate. *Energies* **2020**, *13*, 4925. [CrossRef]
57. Badenes, B.; Mateo Pla, M.Á.; Lemus-Zúñiga, L.G.; Sáiz Mauleón, B.; Urchueguía, J.F. On the Influence of Operational and Control Parameters in Thermal Response Testing of Borehole Heat Exchangers. *Energies* **2017**, *10*, 1328. [CrossRef]
58. Witte, H.J.L. Error analysis of thermal response tests. *Appl. Energy* **2013**, *109*, 302–311. [CrossRef]
59. Lamarche, L.; Raymond, J.; Koubikana Pambou, C.H. Evaluation of the Internal and Borehole Resistances during Thermal Response Tests and Impact on Ground Heat Exchanger Design. *Energies* **2018**, *11*, 38. [CrossRef]
60. Kurevija, T.; Strpić, K.; Koščak-Kolin, S. Applying Petroleum the Pressure Buildup Well Test Procedure on Thermal Response Test—A Novel Method for Analyzing Temperature Recovery Period. *Energies* **2018**, *11*, 366. [CrossRef]

61. Jensen-Page, L.; Loveridge, F.; Narsilio, G.A. Thermal Response Testing of Large Diameter Energy Piles. *Energies* **2019**, *12*, 2700. [CrossRef]
62. Schwarz, H.; Badenes, B.; Wagner, J.; Cuevas, J.M.; Urchueguía, J.; Bertermann, D. A Case Study of Thermal Evolution in the Vicinity of Geothermal Probes Following a Distributed TRT Method. *Energies* **2021**, *14*, 2632. [CrossRef]
63. Sáez Blázquez, C.; Piedelobo, L.; Fernández-Hernández, J.; Nieto, I.M.; Martín, A.F.; Lagüela, S.; González-Aguilera, D. Novel Experimental Device to Monitor the Ground Thermal Exchange in a Borehole Heat Exchanger. *Energies* **2020**, *13*, 1270. [CrossRef]
64. Bae, S.M.; Nam, Y.; Choi, J.M.; Lee, K.H.; Choi, J.S. Analysis on Thermal Performance of Ground Heat Exchanger According to Design Type Based on Thermal Response Test. *Energies* **2019**, *12*, 651. [CrossRef]
65. Serageldin, A.A.; Radwan, A.; Sakata, Y.; Katsura, T.; Nagano, K. The Effect of Groundwater Flow on the Thermal Performance of a Novel Borehole Heat Exchanger for Ground Source Heat Pump Systems: Small Scale Experiments and Numerical Simulation. *Energies* **2020**, *13*, 1418. [CrossRef]
66. Park, S.; Lee, S.; Lee, H.; Pham, K.; Choi, H. Effect of Borehole Material on Analytical Solutions of the Heat Transfer Model of Ground Heat Exchangers Considering Groundwater Flow. *Energies* **2016**, *9*, 318. [CrossRef]
67. Sakata, Y.; Katsura, T.; Serageldin, A.A.; Nagano, K.; Ooe, M. Evaluating Variability of Ground Thermal Conductivity within a Steep Site by History Matching Underground Distributed Temperatures from Thermal Response Tests. *Energies* **2021**, *14*, 1872. [CrossRef]
68. Sliwa, T.; Rosen, M.A. Natural and Artificial Methods for Regeneration of Heat Resources for Borehole Heat Exchangers to Enhance the Sustainability of Underground Thermal Storages: A Review. *Sustainability* **2015**, *7*, 13104–13125. [CrossRef]
69. Miglani, S.; Orehounig, K.; Carmeliet, J. Integrating a thermal model of ground source heat pumps and solar regeneration within building energy system optimization. *Appl. Energy* **2018**, *218*, 78–94. [CrossRef]
70. Zhao, Z.; Shen, R.; Feng, W.; Zhang, Y.; Zhang, Y. Soil Thermal Balance Analysis for a Ground Source Heat Pump System in a Hot-Summer and Cold-Winter Region. *Energies* **2018**, *11*, 1206. [CrossRef]
71. Niemann, P.; Richter, F.; Speerforck, A.; Schmitz, G. Desiccant-Assisted Air Conditioning System Relying on Solar and Geothermal Energy during Summer and Winter. *Energies* **2019**, *12*, 3175. [CrossRef]
72. He, Y.; Bu, X. Performance of Hybrid Single Well Enhanced Geothermal System and Solar Energy for Buildings Heating. *Energies* **2020**, *13*, 2473. [CrossRef]
73. Cupeiro Figueroa, I.; Cimmino, M.; Helsen, L. A Methodology for Long-Term Model Predictive Control of Hybrid Geothermal Systems: The Shadow-Cost Formulation. *Energies* **2020**, *13*, 6203. [CrossRef]
74. Mielke, P.; Bauer, D.; Homuth, S.; Götz, A.E.; Sass, I. Thermal effect of a borehole thermal energy store on the subsurface. *Geotherm. Energy* **2014**, *2*, 5. [CrossRef]
75. Haotian, H.; Yimin, X.; Jianquan, L.; Tiecheng, Z.; Yanan, L.; Qian, Z. Thermal characteristics of a seasonal solar assisted heat pump heating system with an underground tank. *Sustain. Cities Soc.* **2020**, *53*, 101910. [CrossRef]
76. Allaerts, K.; Coomans, M.; Salenbien, R. Hybrid ground-source heat pump system with active air source regeneration. *Energy Convers. Manag.* **2015**, *90*, 230–237. [CrossRef]
77. Bo, X.; Xiaoling, C.; Yanping, Y.; Liangliang, S.; Hongwei, W.; Fariborz, H. A novel hybrid energy system combined with solar-road and soil-regenerator: Dynamic model and operational per-formance. *Energy Convers. Manag.* **2018**, *156*, 376–387. [CrossRef]
78. Peel, M.C.; Finlayson, B.L.; McMahon, T.A. Updated world map of the Köppen-Geiger climate classification. *Hydrol. Earth Syst. Sci.* **2007**, *11*, 1633–1644. [CrossRef]
79. Data from the Institute of Meteorology and Water Management. Available online: danepubliczne.imgw.pl/ (accessed on 28 April 2021). (In Polish).
80. Piotrowska-Woroniak, J. Determination of the Selected Wells Operational Power with Borehole Heat Exchangers Operating in Real Conditions, Based On Experimental Test Energies. *Energies* **2021**, *14*, 2512. [CrossRef]
81. Łapa, M. Executive project. In *Reconstruction of the WBiIŚ Building of the Bialystok University of Technology Together with the Construction of An Internal Monitoring Installation under the Project "Improving the Energy Efficiency of the PB Infrastructure Using Renewable Heat Sources", Scope: Construction of the Heat Pump Installation*; Office Technika Grzewcza Solarsystem: Myślenice, Poland, 2014. (In Polish)
82. *Serial Geological Maps of Poland 1:50,000*; Sheet 339–Bialystok (N-34-107-C); Ministry of Environmental Protection Natural Resources and Forestry; Polish Geological Institute; National Research Institute: Warsaw, Poland, 1998. Available online: http://baza.pgi.gov.pl/resources.html?type=map50&id=339 (accessed on 15 May 2021). (In Polish)
83. Bigaj, Z. *Project of Geological Works for Drilling Boreholes to Use Heat from the Earth*; Hydrogeological Company PANGEA: Chrzanów, Poland, 2013. (In Polish)
84. *Earth Energy Designer ver.4.20 Software*; Blocon AB: Lund, Sweden, 2019.
85. Usowicz, B. Estimating the thermal properties of the soil. *Acta Agrophysica* **2002**, *72*, 135–165. Available online: http://users.ipan.lublin.pl/~{}usowicz/pdf/Estimation.pdf (accessed on 14 June 2021). (In Polish)
86. Madejski, J. *The Theory of Heat Transfer*; University Publishing House of the Szczecin University of Technology: Szczecin, Poland, 1998; ISBN 83-87423-47-5. (In Polish)
87. Cengel, Y.A.; Ghajar, A.J. *Heat and Mass Transfer: Fundamentals and Applications*; McGrawHill: New York, NY, USA, 2010; Available online: www.academia.edu/37959323/Yunus_A_%C3%87engel_Heat_and_mass_transfer (accessed on 10 June 2021).

88. Jarmoc, W. *Technical Design of the Multi-Point Temperature Measurement and Monitoring System*; Elektrokomplex Company: Białystok, Poland, 2014. (In Polish)
89. Piotrowska-Woroniak, J. Preliminary results of the temperature distribution measurements around the vertical ground heat exchangers tubes. *Ecol. Chem. Eng.* **2020**, *27*, 509–528. [CrossRef]
90. Port, P.C. *Guidelines for Designing, Realization and Receiving Installations Powered by Heat Pumps*; Part 1; Polish Organization for the Development of Heat Pump Technology: Cracow, Poland, 2013. (In Polish)
91. Kupiec, K.; Larwa, B.; Komorowicz, T.; Neupauer, K. Temperature profiles in the ground with heterogeneous physical properties. *Chem. Eng. Appar.* **2015**, *54*, 332–333. Available online: http://inzynieria-aparatura-chemiczna.pl/pdf/2015/2015-6/InzApChem_2015_6_332-333.pdf (accessed on 28 July 2021). (In Polish)
92. Rybach, L.; Sanner, B. Ground-source heat pump systems the European experience. *GHC Bull* **2000**, *21*, 16–26. Available online: http://www.sanner-geo.de/media/art4.pdf (accessed on 10 June 2021).
93. Szulgowska-Zgrzywa, M.; Fidorów-Kaprawy, N. Performance analysis of a brine-to-water heat pump and of its boreholes' temperature change during three years of operation. *Appl. Therm. Eng.* **2017**, *127*, 233–244. [CrossRef]
94. Piotrowska-Woroniak, J.; Załuska, W. Variability of Soil Temperatures During 5 Years of a Horizontal Heat Exchanger Operation Co-Operating with a Heat Pump in a Single-Family House. In *Renewable Energy Sources: Engineering, Technology, Innovation: ICORES 2017*; Springer International Publishing: Cham, Switzerland, 2018; pp. 161–175. ISSN 2352-2534/2018.
95. Larwa, B. Heat Transfer Model to Predict Temperature Distribution in the Ground. *Energies* **2019**, *12*, 25. [CrossRef]
96. Bryś, K.; Bryś, T.; Sayegh, M.A.; Ojrzyńska, H. Subsurface shallow depth soil layers thermal potential for ground heat pumps in Poland. *Energy Build.* **2018**, *165*, 64–75. [CrossRef]
97. Karabetoglu, S.; Ozturk, Z.F.; Kaslilar, A.; Juhlin, C.H.; Sisman, A. Effect of layered geological structures on borehole heat transfer. *Geothermics* **2021**, *91*, 102043. [CrossRef]